Glioblastoma and other intracranial tumors elicit systemic sympathetic hyperactivity that limits immunotherapeutic responses

Selena J. Lorrey[+1,2], Lucas P. Wachsmuth[+2,3,4], John B. Finlay[4,5], Corey Neff[6], Katayoun Ayasoufi[6,9], Jessica Waibl Polania[2,3], Alexandra Hoyt-Miggelbrink[2,3], Mackenzie Price[6], Lindsay Rein[8], Samuel Dell[8], Rachael Reesman[6], Xiuyu Cui[2,6], Amelia Hawley[7], Emily Lerner[2,4,11], Daniel Wilkinson[2,6,9], Ethan Srinivasan[2,12], Kyle M. Walsh[6,9], Anoop Patel[6,9,10], Quinn T. Ostrom[6,9], Peter E. Fecci*[1,2,3,6,9,11]

[+]contributed equally
*corresponding author peter.fecci@duke.edu

1. Department of Integrative Immunobiology, Duke University, Durham, NC, USA
2. Brain Tumor Immunotherapy Program, Duke University, Durham, NC, USA
3. Department of Pathology, Duke University, Durham, NC, USA
4. Medical Science Training Program, Duke University, Durham, NC, USA
5. Department of Cell and Molecular Biology, Duke University, Durham, NC, USA
6. Department of Neurosurgery, Duke University, Durham, NC, USA
7. Duke University, Durham NC, USA
8. Department of Medicine, Duke University, Durham, NC, USA
9. Preston Robert Tisch Brain Tumor Center, Duke University, Durham, NC, USA
10. Center for Advanced Genomic Technologies, Duke University, Durham, NC, USA
11. Department of Biomedical Engineering, Duke University, Durham, NC, USA
12. School of Medicine, Duke University, Durham, NC, USA

Author Contributions:
SJL and LPW conceived and designed experiments. SJL, LPW, KA, JWP, AHM, XC, AH, LR, RR, acquired data. SJL, LPW, JBF, KA, SD, MP, CN, QTO analyzed data. SJL, LPW and PEF interpreted data. SJL, LPW, CN, QTO, and PEF wrote the manuscript. EL, DW, ES, KMW, AP provided feedback.

Acknowledgements:
Dr. Fecci is the recipient of a CRI Arash Ferdowsi Lloyd J. Old STAR grant, which helped to fund this work. We thank Gary Archer from the Duke University Brain Tumor Center for providing human serum samples. We further thank Amanda van Swearingen from the Duke University Center for Brain and Spine Metastases for IRB protocol assistance. We thank the Duke University School of Medicine for the use of the Microbiome Core Facility that provided the Nanostring Gene Expression service. This study used the linked SEER-Medicare database, and we thank Zhen Liu for her assistance with data analysis. The interpretation and reporting of these data are the sole responsibility of the authors. The authors acknowledge the efforts of the National Cancer Institute; Information Management Services (IMS), Inc.; and the Surveillance, Epidemiology, and End Results (SEER) Program tumor registries in the creation of the SEER-Medicare database. The collection of cancer incidence data used in this study was supported by the California Department of Public Health pursuant to California Health and Safety Code Section 103885; Centers for Disease Control and Prevention's (CDC) National Program of Cancer Registries, under cooperative agreement 1NU58DP007156; the National Cancer Institute's Surveillance, Epidemiology and End Results Program under contract HHSN261201800032I awarded to the University of California, San Francisco, contract HHSN261201800015I awarded to the University of Southern California, and contract HHSN261201800009I awarded to the Public Health Institute. The ideas and opinions expressed herein are those of the author(s) and do not necessarily reflect the opinions of the State of California, Department of Public Health, the National Cancer Institute, and the Centers for

Disease Control and Prevention or their Contractors and Subcontractors. Schematics in Fig.1, 3 and 4 were created with BioRender.com.

ABSTRACT

Intracranial tumors present unique challenges for immunotherapy. These can include both local and systemic modes of immune suppression whose mechanistic underpinnings are incompletely understood. Here, we reveal that tumors harbored intracranially elicit systemic increases to circulating catecholamine levels, with the resultant chronic sympathetic hyperactivity driving T cell dysfunction and limiting immunotherapeutic success. Conversely, treatment with β-adrenergic blockade increases NF-κB activity in immune cells**,** restores T cell polyfunctionality, modifies the tumor microenvironment, and licenses immune-based therapies in murine models of glioblastoma (GBM) to extend survival. Extended survival is also observed in GBM patients having received β-adrenergic blockade, as well as in patients with melanoma and lung cancer brain metastases who received β-blockade alongside concomitant immune checkpoint inhibition. While β-blockade also impacts outcomes in the setting of extracranial disease, the benefits are especially pronounced in patients harboring intracranial disease burdens. These data suggest that sympathetic hyperactivity facilitates systemic immune dysfunction in the setting of intracranial tumors, specifically and advance a role for β-adrenergic blockade in licensing immunotherapeutic responses within the intracranial compartment.

INTRODUCTION

Glioblastoma (GBM) is the most common primary brain malignancy and remains nearly uniformly lethal. While modern immunotherapeutic approaches enjoy success against a variety of solid tumors, GBM persists as a notable exception[1-3]. Although GBM remains generally confined to the intracranial compartment, it inflicts a remarkably broad range of systemic immune impairments that contribute to treatment failures. Various modes of T cell dysfunction are prevalent and serve to hinder the antitumor response[4-27]. Additional peripheral immune derangements include lymphopenia, lymphoid organ atrophy, and sequestration of T cells in the bone marrow[4,20-22,26-28]. Many of these derangements are not particular to GBM, but instead accompany various tumors if and when these become situated within the intracranial compartment. Lung, melanoma, and breast cancers can all elicit comparable immune dysfunction, for instance, but only when harbored within the brain[20].

Herein we report that intracranial tumors (but not their peripheral counterparts), elicit dramatic rises in systemic catecholamine levels in both patients and mice, which in turn drive loss of critical T cell functions. This remains true regardless of tumor histology Catecholamine infusions into naïve mice are sufficient to recapitulate the same deficiencies, as are specific β-adrenergic agonists (β2 > β1). β2-adrenergic receptors prove the predominant adrenergic receptor on lymphocytes, and their signaling has been shown to suppress immune cell function via inhibition of nuclear factor kappa B (NF-κB) activity[29-34]. Accordingly, we find that treatment with β-adrenergic receptor blockade increases NF-κB activity in immune cells**,** restores T cell polyfunctionality, modifies the tumor microenvironment (TME), and licenses immune-based therapies in murine models of GBM to newly elicit long-term survival.

Large scale analysis of Medicare data also reveals extended survival in GBM patients having received β-blockade, irrespective of indication. Similar survival benefits are seen in patients with melanoma and lung cancer brain metastases who received β-blockade alongside concomitant

immune checkpoint inhibition (ICI), rather than ICI alone. While β-blockade impacts outcomes in the setting of extracranial disease as well, the benefits are especially pronounced in patients harboring intracranial disease burdens. These data suggest critical roles for increased adrenergic activity in facilitating systemic immune dysfunction in the setting of intracranial tumors and advance a particular role for β-adrenergic blockade in licensing immunotherapeutic responses within the intracranial compartment.

RESULTS

Tumors harbored intracranially elicit rises in circulating catecholamine levels

Investigating a role for the sympathetic nervous system (SNS) in mediating the systemic immune dysfunction observed in patients and mice with GBM, we collected sera and spleens from immunocompetent C57BL/6 mice bearing syngeneic intracranial CT2A glioma (CT2A). This model is widely used and is generally accepted as the syngeneic model that most closely recapitulates the immune microenvironment in human GBM[35]. Systemic catecholamine levels from tumor-bearing mice were compared to those in mice instead receiving sham tumor implantations **(Fig. 1A).** Catecholamine levels were elevated in both the serum **(Fig. 1B)** and spleens **(Fig. 1C)** of mice bearing intracranial CT2A, but corresponding increases were not observed in the tumor **(Extended Data Fig. 1 A,B).** Systemic catecholamine rises were observed once a particular tumor size threshold was reached, but further increases in tumor size did not correlate with similar increases in catecholamine levels (**Extended Data Fig. 1 C,D).** Additionally, we assessed corticosterone levels in murine serum and found mixed results (data not shown).

Intrigued, we examined whether rising systemic catecholamine levels might be: 1) particular to GBM; 2) reflective of tumors harbored within the intracranial compartment; or 3) a feature of cancer more broadly. CT2A tumors were injected into either the brains (intracranial, IC) or the flanks (subcutaneous, SubQ) of C57B/6 mice. Systemic elevations in epinephrine and norepinephrine were observed with IC CT2A only, suggesting a phenomenon not particular to GBM, but rather to the intracranial compartment **(Fig. 1D)**. Similar findings accompanied intracranial adaptations of Lewis Lung carcinoma (LLC) and B16 melanoma, but not their peripherally-introduced counterparts, further evidence of an intracranial tumor phenomenon **(Figs. 1E,F)**.

Having observed the above in murine models, we sought to determine whether similar findings might characterize patients. Thus, we examined serum catecholamine levels in patients with either newly diagnosed (n=5) or recurrent (n=10) GBM, as well as in sex-matched healthy controls **(Fig. 1G)**. GBM patients from each cohort exhibited significant elevations in circulating levels of both epinephrine and norepinephrine (**Fig. 1H, I)**. Similar rises were not observed in levels of stress hormones (data not shown).

β2-adrenergic receptors predominate within the intracranial TME, as well as on circulating immune cells

Epinephrine and norepinephrine signal through α- and β-adrenergic receptors. Given the observed rise in catecholamine levels, we examined the relative prevalence of the various α- and β-adrenergic receptor subtypes within the intracranial TME, as well as on circulating immune cells. Publicly available single cell RNA sequencing (scRNAseq) datasets were interrogated and the expression of α-and β-adrenergic receptor subtypes analyzed on tumor cells, as well as on circulating and tumor-infiltrating immune populations. A dataset was

generated by integrating scRNAseq data from human samples that included normal brain (n=5), newly-diagnosed GBM (n=24), recurrent GBM (n=17), low grade glioma (n=2), melanoma brain metastasis (n=8), breast cancer brain metastasis (n=3), lung cancer brain metastasis (n=3), healthy donor peripheral blood mononuclear cells (PBMC) (n=2), and PBMC from patients with GBM (n=5) **(Fig. 2A; Supplementary Fig. 1)**. Healthy brain tissue was also assessed in isolation **(Supplementary Fig. 2)**. After performing quality control, normalization, and integration, this dataset ultimately consisted of 552,442 cells. Clustering was performed and cells were visualized by Uniform Manifold Approximation and Projection (UMAP), yielding cell type-specific clusters that included tumor-, immune-, and brain-resident-cells **(Fig. 2B)**. Examination of clustering by patient **(Supplementary Fig. 1A)** and by tissue of origin **(Supplementary Fig. 1B)** demonstrated successful integration, with no evidence of batch effects. Clusters were identified and annotated according to their expression of signature population-defining genes.

Healthy donor PBMC profiles were found to consist of mainly myeloid and lymphoid clusters **(Fig. 2C),** which predominantly expressed the β2-adrenergic receptor (*ADRB2*). Low expression levels of β1-adrenergic receptors (*ADRB1*) were also seen, while expression of α- and β3-adrenergic receptors was negligible **(Fig. 2D)**. Lymphoid cells demonstrated significantly higher expression of *ADRB2* than myeloid cells **(Fig. 2E)**. PBMCs from patients with GBM yielded comparable findings **(Fig. 2F-H)**.

Repeating these analyses on tumor samples, clustering of newly diagnosed and recurrent GBM samples each revealed population subsets corresponding to tumor cells, microglia, myeloid cells, and lymphoid cells **(Fig. 2I)**. More in-depth analysis of immune compartments in PBMCs and tumor-infiltrating immune cells can be found in **Supplementary Figs. 4 and 5.** Feature plots demonstrated that the β2-adrenergic receptor was again the predominant adrenergic receptor present across all clusters, with minimal to negligible expression of the other receptor subtypes observed **(Fig. 2J and Supplementary Fig. 3)**. Likewise, lymphoid, myeloid, and microglial cells were the highest expressers of the β2-adrenergic receptor, while receptor expression was essentially absent on tumor cells **(Fig. 2K)**. Similar findings were uncovered in brain metastases **(Fig. 2L-N),** though the GBM TME appears to express higher levels of the β2-adrenergic receptor, particularly within the lymphoid compartment. β2-adrenergic receptor expression within the TME of murine CT2A gliomas was likewise confirmed by immunofluorescence **(Supplementary Fig. 6)**

Examination of feature plots of adrenergic receptor expression in healthy brain tissue demonstrated minimal expression of all receptors except for α1 (*ADRA1A* and *ADRA1B*), which was found to be concentrated in neurons and astrocytes (**Supplementary Fig. 2A**). While expression levels of β-adrenergic receptors in healthy brain were found to be quite low, comparison of the relative expression of β1- and β2-adrenergic receptors specifically indicated that astrocytes and microglia, respectively, were the cell populations with the highest expression of these two receptors (**Supplementary Fig. 2B)**.

Systemic T cell function is impaired by β-adrenergic signaling but is restored by β-adrenergic blockade in the setting of intracranial tumors

We next sought to evaluate the contribution of elevated catecholamine levels to T cell dysfunction, which has been extensively characterized in the context of GBM. Historically, studies have reported diminished T cell reactivity, often demonstrating limited proliferative and cytokine responses [4-6,8,9,14,16-19,24,26,27,36-42]. More current techniques assess multiple cytokines

simultaneously to address T cell "polyfunctionality",[43-54] which has been linked to outcomes in various tumor types[55-57].

We thus began by using a high-throughput, single-cell proteomics assay that detects cytokine secretion at the single-cell level. Splenic T cells from mice under each experimental condition were isolated and stimulated *ex vivo* with anti-CD3/anti-CD28 antibodies for 48 hours. Individual T cell production of Granzyme B, IFNγ, MIP-1α/CCL3, IP-10/CXCL10, RANTES/CCL5, IL-27, sCD137/4-1BB, IL-21, IL-17 and IL-6 was assessed and the proportion of T cells exhibiting polyfunctional cytokine production (2 or more cytokines) measured **(schematic in Fig. 3A).** In this single-cell proteomics assay, cytokine secretion was analyzed from individual cells. For validation, portions of the assay were performed twice, and representative data are shown. Flow cytometric validation of individual cytokines (Granzyme B, IFNγ) was also performed, and some of these data appear in subsequent figure panels. **Extended Figure 2A** tabulates the cytokines measured and catalogues the number of cells passing quality control (QC) for initial and repeat assays.

The assay was employed to assess T cell polyfunctionality (the capacity of individual T cells to produce multiple pro-inflammatory cytokines) and to compare systemic (splenic) T cell function in the setting of either peripheral or intracranial tumor. Likewise, naïve mice were implanted with slow-release pumps and infused systemically with either a mixture of epinephrine/norepinephrine or the β2-agonist salbutamol in order to assess the sufficiency of adrenergic stimulation for eliciting compromises to T cell function (β2-agonism was chosen given the predominance of *ADRB2* expression detected within lymphoid populations above). CT2A gliomas elicited a greater decline in systemic $CD8^+$ T cell function when situated intracranially, a decline that was likewise recapitulated by infusion of either catecholamines (epi/norepi) or salbutamol into naïve mice. In the context of intracranial CT2A, epi/norepi, or salbutamol, no T cells secreted more than 3 pro-inflammatory cytokines, a loss of function unique to these conditions **(Fig. 3B).** To validate at the single cytokine level and permit statistical comparisons, we examined Granzyme B production by $CD8^+$ T cells. As the violin plot in **Fig. 3C** demonstrates, systemic Granzyme B production significantly declined in the setting of intracranial CT2A, epi/norepi, or salbutamol, but not subcutaneous CT2A.

A recent paper has suggested that the β1-adrenergic receptor, although not prevalent on T cells, may nonetheless be linked to T cell dysfunction[58]. Therefore, to better assess the relative contributions of both β1- and β2-adrenergic agonism to T cell dysfunction, we again implanted slow-release pumps into naïve, non-tumor-bearing (NTB) mice, this time infusing either the β1-selective agonist dobutamine or the β2-selective agonist salbutamol. Only salbutamol led to a decline in T cell Granzyme B production **(Fig. 3D)**, but both dobutamine and salbutamol severely impaired production of IFNγ **(Fig. 3E).** Salbutamol likewise elicited a reduction to the proportion of polyfunctional T cells secreting both Granzyme B and IFNγ **(Fig. 3F)**. T cell proliferation was also assessed by staining for Ki67. Only salbutamol led to a significant decline in $Ki67^+$ T cells **(Fig. 3G)**, although there was a trend toward reduced proliferation in the $CD8^+$ compartment of mice treated with dobutamine, as well **(Fig. 3H)**.

Given the observed impact of both β1- and β2-adrenergic agonism, we opted to evaluate the impact of treating tumor-bearing mice with the readily translatable nonselective β-adrenergic antagonist, propranolol. Treatment with propranolol partially restored polyfunctional T cell responses and Granzyme B production in mice with intracranial CT2A (**Fig. 3I,J).** The splenic $CD3^+$, $CD4^+$ non-Treg, and $CD8^+$ T cell compartments all exhibited higher expression of the proliferation marker Ki67 (**Fig. 3 K-M)** and increases (or trending increases) in the proportion of

cells with a central memory phenotype **(Extended Data Fig. 3B,C)**. Propranolol did not prevent systemic immune derangements such as lymphoid organ atrophy, T cell sequestration, or lymphopenia **(Extended Data Fig. 3)**, and there were no significant differences elicited to the overall immune composition of the various lymphoid compartments **(Supplementary Fig. 7).**

β-adrenergic blockade proffers a pro-inflammatory intracranial TME

Having examined the impact of β-adrenergic blockade on systemic T cell function, we then turned to the local TME. Many of the proinflammatory cytokines impacted by adrenergic activity above (Granzyme B, IFNγ, MIP-1α/CCL3, sCD137/4-1BB, and RANTES/CCL5) are regulated by NF-κB. Interestingly, β2-adrenergic receptor signaling is known to suppress NF-κB activity and thus inhibit inflammatory responses in the setting of other intracranial pathologies, such as stroke[59]. We therefore sought to understand the impact of β-adrenergic blockade within the intracranial TME, as well as to investigate any influence on NF-κB-mediated immune activity. Mice with intracranial CT2A were administered either 0.5g/L propranolol or vehicle control in drinking water *ad libitum* beginning on the day of tumor implantation (Day 0). Upon clinical decline, intracranial tumors were harvested for analysis and $CD45^+$ immune cells were positively selected for western blot analysis. In order to assess for differences in NF-κB at the protein level, we examined the expression of p65, the most abundant NF-κB subunit[60]. Higher levels of p65 protein expression were seen in CT2A-bearing mice treated with propranolol **(qualitative Fig. 4A; quantitative data Fig. 4B).**

In order to further query for differences in NF-κB levels among tumor-infiltrating in immune cells, we sorted $CD45^+$ cells from the TME, enriched for either T cells or APCs, and then performed bulk RNA-sequencing **(schematic in Fig. 4C).**

Indeed, T cells from tumors of mice treated with propranolol harbored significantly decreased *Nfkbia* (IkBα) transcript levels and, likewise, a striking increase in IL-2 transcript levels **(Fig. 4D).** IkBα is the "inhibitor of NF-κB" that is degraded upon activation of the canonical NF-κB signaling pathway[61]. IL-2 is a canonical downstream target of NF-κB**.** Together, these data support an increase in NF-kB activity in T cells within the intracranial TME**.** As NF-κB activation is required for T cell priming[62], we also assessed downstream NF-κB target genes in the APC-enriched samples and observed increases in transcript levels of the NF-κB subunits c-Rel and Relb **(Fig. 4E),** as well as CD40, IL-12a and CD80 **(Fig. 4F),** all of which are expressed by dendritic cells (DCs)**.**

Phenotypic changes to immune cells within the TME were also assessed via flow cytometry **(schematic in Fig. 4G; Gating strategy in Supplementary Fig. 8).** Treatment with propranolol increased the number of tumor-infiltrating immune cells overall **(Fig. 4H).** These increases were driven by increased numbers of $CD8^+$ T cells **(Fig. 4I)** and conventional type 1 dendritic cells (cDC1s), which are critical for T cell priming and $CD8^+$-mediated cytotoxicity[63,64] **(Fig. 4J**). Accordingly, there were also more $CD8^+$ T cells that produced Granzyme B in the TME of mice treated with β-adrenergic blockade (**Fig. 4K).** No differences in the proportion or number of migratory or resident cDC1s were observed (**Supplementary Fig. 10).**

Examining CD40 expression on cDC1s as a surrogate for T cell priming capacity, we found that propranolol increased both the frequency and intensity of CD40 expression on cDC1s in the TME **(Fig 4. L,M).** The same was true for CD40L on T cells, facilitating their interaction with $CD40^+$ DCs (**Fig. 4N,O**). Upregulation of both CD40 and CD40L requires NF-κB activation[65,66]. The TME of mice treated with propranolol also harbored significantly fewer $CD206^+$

immunosuppressive "M2-like" macrophages, with no concomitant in the percentage of iNOS^{+} inflammatory "M1-like" macrophages **(Fig. 4O-Q; Gating strategy in Supplementary Fig. 9).**

As T cell exhaustion is an established form of T cell dysfunction in the TME[67,68] that may in turn be influenced by β1-adrenergic activity[58], we evaluated the impact of β-adrenergic blockade on T cell differentiation states. In propranolol-treated mice, there was a slight trend among tumor-infiltrating CD8^{+} T cells towards a progenitor exhaustion phenotype (CD44^{+}PD1^{+}SLAMF6^{+}TIM3^{-}), but no difference in the prevalence of terminally exhausted cells (CD44^{+}PD1^{+}SLAMF6^{-}TIM3^{+}) **(Extended Data Fig. 4A,B)**. Likewise, while transcript levels of the classical exhaustion markers *Lag3*, *Havcr2* (Tim3) and *Pdcd1* (PD-1) trended lower in mice treated with propranolol, there was no significant difference between the groups **(Extended Data Fig. 4C)**.

Treatment with β-adrenergic blockade enhances the response to immunotherapy in mice and patients with intracranial tumors

Having observed benefits to both systemic and local immune functions, we next examined whether β-adrenergic blockade might improve immunotherapeutic responses to intracranial tumors and meaningfully prolong survival. We first employed a CT2A glioma model engineered to overexpress the tumor-associated rejection antigen TRP2 (CT2A-TRP2). Mice with intracranial CT2A-TRP2 were administered either propranolol (initiated day 0); a 4-1BB agonist (on days 9, 12, 15, and 18); or the combination. The combination treatment provided a survival benefit when compared to no treatment, propranolol alone, or 4-1BB agonist alone (**Fig. 5A**). Similar patterns of survival were seen in a more stringent CT2A model that lacked a homogenous rejection antigen **(Fig. 5B).** Impact on tumor growth curves, specifically, was confirmed using a model of CT2A-luciferase and assessing tumor progression with bioluminescence imaging (BLI). Decreased rates of tumor growth were indeed observed in the combination group **(Extended Data Fig. 5).** Notably, no significant survival differences were observed between initiation of propranolol at day 0 compared to day 7, suggesting that β-adrenergic blockade can enhance immunotherapeutic responses in the context of established tumor **(Extended Data Fig. 6)**. For additional comparison, we also evaluated the impact of blocking the hypothalamic-pituitary-adrenal (HPA) axis with anti-corticotropin-releasing hormone (anti-CRH). No survival benefit was seen alone or in combination with immunotherapy (**Supplementary Fig. 11**).

The studies above were conducted with 4-1BB agonism, given the documented capacity to elicit a modest anti-tumor immune response against glioma[69]. We now inquired, however, whether β-adrenergic blockade might also be capable of licensing a response to anti-PD1 therapy, to which human GBM and murine CT2A have both been notoriously resistant[1,20,26,69,70]. The combination of propranolol and anti-PD1 indeed resulted in long-term survival, while neither therapy alone produced such therapeutic impact **(Fig. 5C)**.

To assess the significance of these findings to patients, we utilized the Surveillance, Epidemiology and End Results (SEER)-Medicare database to first retrospectively assess the impact of β-blockade therapy (prescribed for any indication) on outcome in patients with GBM (treatment codes outlined in **Supplementary Table 1**). As no immunotherapies are currently FDA-approved in GBM, they are not insurance-reimbursed and thus no data on the combination of β-blockade and immunotherapy are currently available through the SEER-Medicare database. We were, however, able to assess the impact of β-blockade monotherapy in patients with GBM. For the purposes of this retrospective study, a total of 8,743 patients met criteria, including the intrinsic criterion age > 65 (patients <65 are not recorded in Medicare data, unless they possess specific co-morbidities). Medicare patients enrolled due to end-stage renal

disease or disability were excluded. Patients enrolled in a health maintenance organization (HMO) 6 months prior to and 12 months after primary diagnosis were also excluded (see demographics in **Table 1.1)**. Of these 8,743 patients, 655 had been prescribed β-adrenergic blockade at the time of their cancer diagnosis. Median overall survival (OS) of GBM patients receiving β-adrenergic blockade (12 months) was more than 200% that of those not receiving β-adrenergic blockade (5 months) (HR 0.63; 0.57, 0.69 95% CI; p<0.0001) **(Fig. 5D; Table 1.2, 1.3)**.

In contrast to GBM, checkpoint blockade is FDA-approved in patients with brain metastases arising from melanoma and from certain lung cancers, permitting us to identify patients with these conditions who may have been treated with checkpoint blockade and β-adrenergic blockade either concomitantly or individually. We therefore returned to the SEER-Medicare database to retrospectively determine survival outcomes in patients with melanoma or lung cancer brain metastases who had received checkpoint blockade alone for their cancer versus those who had received checkpoint blockade concomitantly with β-adrenergic blockade (the latter again for any indication). Survival was also assessed in patients who received β-adrenergic blockade alone (for any indication), as well as in those who received neither β-adrenergic blockade nor checkpoint blockade.

A total of 25,711 lung cancer patients and 2,332 melanoma patients, all diagnosed with concomitant brain metastases, were assessed **(Fig. 5E).** Beginning with lung cancer, we evaluated outcomes in patients with brain metastasis who met the inclusion criteria described previously. Patients receiving no β-blocker and no immune checkpoint blockade (n=20,905) had a median OS of 6 months, while those receiving a β-blocker alone (n=3,733) had a longer median OS of 10 months (p<0.001). Patients receiving checkpoint blockade alone (n=806) exhibited a median OS of 19 months, while those prescribed both a β-blocker and checkpoint blockade (n=267) had a median OS of 25 months, which represented a > 30% increase (25 months vs. 19 months, p=0.013). Patients receiving both therapies also survived >150% longer than those that received β-blocker alone (25 months vs. 10 months, p<0.001) and >300% longer than those patients that received neither β-blocker nor checkpoint blockade (25 months vs. 6 months, p<0.001) **(Fig. 5F; Table 2). Table 2.4** demonstrates the hazard ratios (HR) for comparisons amongst groups.

We next evaluated outcomes in melanoma patients with brain metastasis as above. Of the 2,332 patients included, 1,531 patients received neither β-blocker nor checkpoint blockade and exhibited a median OS of 17 months, while patients that received β-blocker only (n=215) exhibited a median OS of 28 months (28 months vs. 17 months, p<0.001). Patients who received checkpoint blockade alone exhibited a median OS of 32 months, while the 139 patients who were prescribed both a β-blocker and checkpoint blockade exhibited a median OS of 52 months (52 months vs. 32 months, p=0.006). This represents a >60% increase in median OS in patients who received both β-blockade and checkpoint blockade compared to checkpoint blockade alone and a >200% increase compared to those patients that received neither β-blocker nor checkpoint blockade (52 months vs. 17 months, p<0.001) **(Fig. 5G; Table 3)**. **Table 3.4** demonstrates the hazard ratios (HR) for comparisons amongst groups.

β-adrenergic receptor expression has been seen on melanoma[71-74] and other cancers,[74-77] with a direct role in tumor progression reported. In melanoma, in particular, studies suggest that combination β-adrenergic and checkpoint blockade may promote extended recurrence-free survival in the absence of intracranial disease.[72,78] Given our findings of increased adrenergic activity in the setting of intracranial tumors, specifically, we looked to establish the relative

potency of β-adrenergic blockade for licensing immunotherapeutic responses when intracranial disease was present versus not. Finally, then, we examined the effects of concomitant β-blocker and checkpoint blockade in metastatic lung cancer and metastatic melanoma patients who had no brain metastases (metastatic extracranial disease only, at diagnosis). Median OS among lung cancer patients who received combination β-blocker and checkpoint blockade therapy in the setting of extracranial disease only was 22 months vs. 18 months among those who received checkpoint blockade only ($p<0.001$). This represented a modest ~20% increase (respective increase in the setting of intracranial disease was 32%) **(Fig. 5H and Table 4.3)**. Median survival in patients with exclusively extracranial melanoma in the combination group was 35 months compared to 27 months in those who only received checkpoint blockade (~30% increase), although this difference was not statistically significant **(Fig. 5I; Table 5.3)** (respective increase in the setting of intracranial disease was 63%, $p=0.006$). In all cohorts, the cause of death for the majority of patients was their cancer (**Supplementary Fig. 12).** Thus, while β-blockade also impacts outcomes in the setting of extracranial disease, the benefits are especially pronounced in patients harboring intracranial disease burdens.

DISCUSSION

The intracranial compartment proffers a unique set of challenges that can serve to limit immunotherapeutic efficacy. Treatment failures have been especially prominent in the context of GBM. Historical impediments include the blood-brain barrier (BBB)[26,79-81]; challenges to T cell priming and function[82-85] and a heavily immunosuppressive TME[22,26,37,82-88]. Furthermore, despite rarely leaving its intracranial confines, GBM is known to suppress systemic immune function. Much of this depressed systemic immune function is not unique to GBM, but instead accompanies pathologies of the intracranial compartment more broadly[20,89]. The mechanistic underpinnings of such systemic restrictions to immune function and their implications for immunotherapeutic success remain largely unexplored[90]. Herein we reveal that tumors of the intracranial compartment, uniquely, elicit steep rises in systemic catecholamine levels that are sufficient to restrict both local and systemic immune function. Conversely, treatment with nonselective β-adrenergic blockade increases NF-κB activity in immune cells**,** restores T cell polyfunctionality, modifies the TME, and licenses immune-based therapies in murine models of GBM.

The immunosuppressive effects of sympathetic activity are well-documented[91-94]. Likewise, elevated systemic catecholamine levels have been described in the setting of other intracranial pathologies, such as stroke, where they are an identified component of “stroke-induced immunodepression syndrome” (SIDS)[95]. Studies suggest that SIDS may be attributable to inhibition of NF-κB activity following β-adrenergic signaling[96]. Our data suggest that a similar immunosuppressive axis may be active in the context of intracranial tumors as a result of chronic sympathetic hyperactivity. Notably, we observe dramatic catecholamine rises in the spleen and in circulation, but not in the TME. These data suggest that the chronic sympathetic hyperactivity arises from triggering of a systemic sympathetic response, and not simply local production of catecholamines within the tumor. Additionally, there was a relative lack of adrenergic receptor expression found on human GBM cells, with higher expression found on both systemic and tumor-infiltrating immune cells. Consequently, β-adrenergic blockade likely acts predominantly on the systemic immune compartment. Further investigation into the immediate upstream determinants of sympathetic hyperactivity in the setting of intracranial tumors is warranted.

Our data demonstrate that both β1- and β2-adrenergic signaling likely play a role in contributing to catecholamine-induced immune dysfunction, although β2-adrenergic receptors are the more prevalent receptor subtype on systemic immune cells and within the TME. A recent publication has advanced a role for the β1-adrenergic receptor in promoting T cell exhaustion[58], yet also found that the greatest improvements to immune responses in extracranial tumors were seen with nonselective (rather than β1-specific) adrenergic blockade[58]. Our results are in accordance with these findings and, together, serve to highlight contributions from both receptors.

Other studies investigating the effects of β-adrenergic signaling on immunity align with the data presented herein. One such study denoted that β-adrenergic signaling disrupts NF-κB pathways and CD40 signaling in dendritic cells in a manner that was similarly reversed by treatment with propranol[97]. Another group described the myeloid-directed anti-tumor activity of an α2 adrenergic agonist, although the authors examined extracranial tumors only[98]. Two additional studies highlighted the ability of β-adrenergic blockade to mitigate either the number[99] or activity[100,101] of immunosuppressive myeloid cells within the TME, much as we observed as well.

β-adrenergic receptor expression has been detected on melanoma[71-74] and other cancers[74-77], with a direct role in tumor progression suggested. As a result, β-adrenergic blockade has been previously investigated in peripheral cancers for its direct antitumor effects as a monotherapy[72,102,103], with conflicting results[104-107]. Further, several studies have examined the direct inhibitive effects of propranolol on glioma cell lines *in vitro* (predominantly rat)[108-111], although our data reveal relatively low expression of β-adrenergic receptors on glioma cells compared to the immune compartment. Studies in peripheral cancers have examined the local immune impact of adrenergic signaling within the TME[102,103], generally positing a role promoting T cell exhaustion[58,101,112-115]. We, however, report a larger array of β-adrenergic-mediated immune deficits amidst intracranial cancers, which are likely attributable to the chronic systemic sympathetic hyperactivity that we also uncover in the context of these tumors. Such chronic sympathetic hyperactivity also quite likely explains the added benefit to β-adrenergic blockade seen in the intracranial tumor setting.

Our study reports extended survival in GBM patients having received β-adrenergic blockade, as well as in patients with melanoma and lung cancer brain metastases who received β-blockade alongside concomitant ICI. While β-blockade also impacts outcomes in settings of exclusively extracranial disease, the benefits are especially pronounced in patients harboring an intracranial disease burden. Our studies examining patients with brain metastases are particularly relevant, as brain metastases are now 10 times more prevalent than GBM, with lung cancer and melanoma exhibiting two of the highest rates of intracranial metastasis[116,117]. In melanoma, studies have previously examined the combination of β-adrenergic and checkpoint blockade[72,78], but these have frequently excluded patients with stage IV disease, and thus, brain metastases[101,118-120]. One study has previously investigated the impact of β-adrenergic blockade in the setting of GBM, assessing outcomes retrospectively in patients with recurrent GBM (n=243) and revealing no association between β-blockade and overall survival[121]. In contrast, our analysis of the SEER-Medicare database investigated a cohort of 8743 GBM patients (35x larger) and included those who were newly diagnosed.

In our analysis of the SEER-Medicare data, we attempted to list all reasonable exclusions. The nature of retrospective data, however, is such that it is not possible to account for all potential confounders and caveats remain. Underlying differences in a patient's past medical and diagnostic history could account for a component of the survival benefit associated with β-

blocker usage, as could the impact of β-blockers on those conditions. We would expect some of this variability to be captured in the patient comorbidity score that is included in all multivariate models shown. Additionally, care must be taken when interpreting the use of claims data for metastasis research.[122] Use of ICD-9 or ICD-10 to identify patients with asynchronous brain metastases will be imperfect due the nature of diagnostic claims data as, while SEER-Medicare contains nearly all claims billed through Medicare, previous research has shown that the information contained in the claims themselves is not always reliable or valid.[123-126] Threats to the validity of claims may include under-/over-diagnosing, patient compliance with billed treatments, and inconsistent use of billing codes, among others. Prior evaluations have demonstrated that use of tumor-specific algorithms have ~55% sensitivity and 85% specificity for lung cancer, suggesting that individuals with metastasis will be missed but those assigned as having metastatic disease are likely correctly identified. These algorithms will result in the underestimation of total asynchronous brain metastases.[127] It was also not possible to determine further details of β-blocker usage, beyond their being billed to Medicare. Together, this makes our data, as with all retrospective data, subject to the bias of indication. While our data examining survival in patients with GBM and intracranial metastases are therefore limited in scope by this bias, the prospective complement proffered by our murine survival and immune data strongly suggest a specific benefit to combining β-adrenergic blockade and immunotherapy in the setting of intracranial tumors.

The data presented herein support the initiation of prospective randomized controlled trials to examine the addition of β-adrenergic blockade to immunotherapeutic regimens in patients with intracranial cancers, whether primary or metastatic. Such trials, we anticipate, will be viewed favorably, as β-blockers are FDA-approved, relatively inexpensive, and have exhaustively established safety profiles[128]. Repurposing β-blockers as an immunotherapeutic adjunct may ultimately represent a novel intervention for licensing long sought-after effective immune responses within the intracranial compartment.

METHODS

Mice

The Institutional Animal Care and Use committee (IACUC) at Duke University Medical Center approved all experimental procedures. Female C57BL/6 mice purchased from Charles River Laboratories were purchased at 5-6 weeks of age. Animals were maintained under specific pathogen-free conditions at the Cancer Center Isolation Facility of Duke University Medical Center. All experimental procedures were approved by the IACUC.

Cell lines

Murine CT-2A malignant glioma was kindly provided by Robert L. Martuza (Massachusetts General Hospital, MA, USA). LLC1/2 lung adenocarcinoma were purchased from the American Tissue Culture Collection (ATCC). Murine B16F0 melanoma was obtained from the Duke Cell Culture Facility but is also available from ATCC. All cell lines are syngeneic on the C57BL/6 background. CT-2A and LLC1/2 were grown *in vitro* in Dulbecco's Modified Eagle's Medium (DMEM) with 2mM L-glutamine and 4.5mg ml^{-1} glucose (Gibco) containing 10% fetal bovine serum (FBS) (Sigma). B16F0 cells were grown *in vitro* in DMEM with 4mM L-glutamine, 4.5mg ml^{-1} glucose, 1mM sodium pyruvate, 1500 mg/L sodium bicarbonate containing 10% FBS (Sigma). Cells were collected in the logarithmic growth phase. All cell lines were authenticated and tested negative for mycoplasma and interspecies contamination by IDEXX Laboratories.

Tumor Implantation

For intracranial implantation, tumor cells were resuspended at a given concentration in PBS, then mixed 1:1 with 3% methylcellulose and loaded into a 250μL syringe (Hamilton). Prior to injection, mice were anesthetized with isoflurane and subject to an anteroposterior incision to reveal the skull. The needle was positioned 2mm to the right of the bregma and 4mm below the surface of the skull at the coronal suture using a stereotactic frame. $1e^4$ CT-2A, $1e^3$ B16F0 or $1e^3$ LLC1/2 cells were delivered in a total volume of 5μL per mouse. For subcutaneous implantation, $5e^5$ CT2A, $2.5e^5$ B16F0, or $5e^5$ LLC1/2, were injected in a total of 200μL of PBS into the subcutaneous tissues of the left flank.

Catecholamine and Corticosterone Analysis

De-identified human samples were used in this study with exempt Institutional Review Board (IRB) status granted from the Duke University Health System IRIB (protocol ID: Pro00112766). De-identified serum samples from 5 female and 5 male GBM patients were collected at time of recurrence, processed immediately, and stored in vapor phase liquid nitrogen. De-identified serum samples from 5 newly diagnosed GBM patients (3 males, 2 females) were collected at time of diagnosis, likewise processed immediately, and stored similarly. Serum from patients with both newly-diagnosed and recurrent GBM was collected during a pre-operative clinic visit. Patient serum samples were obtained from patients at Duke University (protocol # Pro00007434, BTBR). De-identified healthy control human serum was obtained from BioIVT (5 males and 5 females, HUMANSRM-0001254 and HUMANSRM-0001253, respectively). Healthy control human serum was obtained according to the BioIVT Standard Operating Procedures. Briefly, after whole blood was drawn into a dry collection bag, it was sun at 4,500-5,000 x g for 10-15min in a refrigerated centrifuge. Supernatant was then transferred into another bag and allowed to clot at room temperature. The resulting material was spun at 3,500-5,000 x g for 15-20min in a refrigerated centrifuge and subsequently aliquoted.

Glioblastoma patient serum was obtained according to the standard operating procedure for clinical samples at Duke University. Briefly, whole blood was allowed to clot for up to 60min then centrifuged at 2200 RPM for 10min at room temperature. Serum was aliquoted and stored at -80C and subsequently transferred to liquid nitrogen for long-term storage.

Blood and spleen were collected from non-tumor bearing mice or mice with intracranial tumors or subcutaneous tumors at respective humane endpoints. To mitigate the differential impact of stress on mice, all mice were handled as minimally as possible and were immediately anesthetized using isoflurane, with only one cage (n=5 mice) handled at any given time. They were then subject to retro-orbital bleed and subsequent euthanasia and tissue harvest. All samples were stored on ice and processed immediately, with total processing time not exceeding 1hr. Serum samples and spleen supernatant from all groups were processed simultaneously. Blood samples were centrifuged at 2000g for 15min at 4°C to isolate plasma, which was isolated in 58.8μL aliquots with 1.2μL 50mM EDTA 200mM sodium metabisulfite per sample to protect against catecholamine degradation. Spleens were collected into 500μL of a PBS/ 50mM EDTA 200mM sodium metabisulfite solution, weighed, homogenized through 70μm filters, washed with an addition 500μL of PBS/EDTA/sodium metabisulfite solution for a total of 1mL, then centrifuged at 500g for 5min at 4°C. Supernatants were collected by combining 58.8μL supernatant and 1.2μL 50mM EDTA 200mM sodium metabisulfite into Eppendorf tubes.

All samples, including human serum samples were stored at -80°C. Epinephrine and norepinephrine levels in plasma, serum, and spleen supernatant were analyzed using the 2-CAT (A-N) Research ELISA (Rocky Mount Diagnostics).

Murine tissue harvest

Tumor, spleen, thymus, inguinal or deep cervical lymph node, and tibia were collected at defined and/or humane endpoints, in accordance with protocol. For intracranial tumor-bearing animals, humane endpoints include inability to ambulate two steps forward with prompting. For subcutaneous tumor-bearing animals, humane endpoints include tumor size greater than 20 mm in one dimension, 2000mm^3 in total volume, or tumor ulceration or necrosis. Spleens, lymph nodes and thymi were weighed. Briefly, tissues were processed in RPMI or PBS, minced into single cell suspensions, cell-strained, counted, stained with antibodies, and analyzed via flow cytometry.

Tumors were mechanically homogenized using a Dounce Tissue Homogenizer and enzymatically digested using 0.05mg ml^{-1} Liberase TL (Roche), 0.2mg ml^{-1} Dnase I (Roche) in HBSS with calcium and magnesium. Tumors in digestion buffer were then incubated at 37°C for 15min, PBS was used to quench the enzymatic reaction, and tumors were filtered (70µm). After centrifugation, cells were resuspended in 1x RBC Lysis Buffer (eBioscience) for 3min and quenched with PBS. Samples were subsequently centrifuged then resuspended in 30% Percoll (Sigma Aldrich) and centrifuged at 500g for 20min at 18°C with a low brake. The myelin-containing supernatant was then aspirated, and the cell pellet resuspended in PBS for staining.

Blood was collected into EDTA tubes and mixed thoroughly to prevent coagulation. After collection, 75µL of each blood sample combined with 1mL 1x RBC Lysis Buffer (eBiosciences) and incubated for 3min then quenched with PBS. RBC lysis was performed twice before proceeding to staining.

Single-cell RNA sequencing analysis

Integration of a single cell atlas and downstream analyses were performed in Python (v3.9.13) using Scanpy (v1.9.1) and scvi-tools (v0.17.4). Filtered feature gene matrices from the following datasets were queried from the gene expression omnibus or provided by the original authors: GSE182109 (2 low grade glioma, 10 newly diagnosed GBM, 5 recurrent GBM)[129], GSE154795 (14 newly diagnosed GBM, 12 recurrent GBM, 5 PBMCs from recurrent GBM, 2 healthy donor PBMCs)[130], GSE160189 (5 normal brain)[131], GSE200218 (5 melanoma brain metastases)[132], and GSE186344 (3 breast cancer brain metastases, 3 lung cancer brain metastases, and 3 melanoma brain metastases)[133].

Matrices were read into Python with sc.read_10x_mtx(), and relevant metadata information was added (patient of origin, study of origin, tumor type). Anndata objects from each dataset were then concatenated with adata.concatenate() with join=outer. QC metrics were calculated and cells with >8000 genes by counts, <500 total counts, and >25 percent mitochondrial DNA were removed. A normalized counts layer for downstream analysis was created with sc.pp.normalize_total(), with a target sum of 10,000. 5000 highly variable genes were selected using scvi.data.poisson_gene_selection() with batch_key=patient of origin, and using the raw counts matrix, as is required for scvi. The model was then constructed using the filtered anndata object containing only highly variable genes with scvi.model.SCVI.setup_anndata(). Again, the raw counts layer was used, with the batch_key set to patient of origin, and percent mitochondrial counts used as continuous categorical covariate. Because we were interested in primarily distinguishing between healthy cells, tumor cells, and immune cells, and not specific tumor types, tumor type was used as a categorical covariate in the model. The model was run with model.train() with an early stopping patience of 20 and 700 maximum epochs. The latent

representation of the model was obtained with model.get_latent_representation() and added to .obsm of the original anndata object (containing all genes). For clustering, nearest neighbors were calculated using the .obsm latent representation from the model and n_neighbors=15, followed by sc.tl.umap() with min_dist=0.5 and sc.tl.leiden() with resolution=2.0. Clusters were analyzed individually with log1p total counts and percent mitochondrial counts. The model tends to cluster low quality cells (high mitochondrial content, high total counts, or low total counts) together, allowing for further quality control, rather than using a strict initial cutoff by QC metrics prior to visualizing data and cell types[134]. Expression of known marker genes from each tumor type, normal cell type, and immune cell components were evaluated by plotting gene expression onto the UMAP, using the normalized counts layer. We also assessed marker genes per leiden cluster with sc.tl.rank_genes_groups(), method=Wilcoxon, using the normalized counts layer. If a leiden cluster had exceptionally high or low total counts, or high mitochondrial counts, and did not align with known tumor, normal cell, or immune marker combinations (by UMAP gene expression and Wilcoxon Rank-Sum cluster markers), it was filtered out as low-quality cells or likely doublets. Each time leiden clusters were removed, another model was retrained with the same parameters, starting at the highly variable gene selection step and progressing through cluster quality control, until there were no clear low quality cell clusters remaining. Notably, in order to minimize bias in downstream analysis, expression of adrenergic receptors was not considered in any of the quality control and filtering steps.

All UMAP plots were generated with sc.pl.umap(), and clusters were annotated manually based on combinations of known marker genes. Matrix plots and Dot plots were generated with sc.pl.matrixplot() and sc.pl.dotplot(), respectively, with the normalized counts layer in both cases. For generating disease specific UMAPs, the global anndata object was subset based on patient metadata, and the primary UMAP embedding was retained to preserve graph architecture, allowing for easier comparison between subset and data objects.

***In vivo* Treatment**

For immunotherapy administration, 200μg 4-1BB agonist or vehicle control was administered intraperitoneally in 200μL PBS every 3 days, beginning at day 9, through day 18 post-tumor implantation for a total of 4 treatments.

For propranolol administration, mice were given 0.5g/L propranolol or vehicle control in drinking water *ad libitum* beginning on the day of tumor implantation.

For epinephrine/norepinephrine, dobutamine (β1-adrenergic receptor agonist) and salbutamol (β2-adrenergic receptor agonist) administration, naïve mice were implanted with subcutaneous osmotic pumps (Alzet) for seven days. Mice received a combination of 10mg/kg/day of epinephrine and 7mg/kg/day of norepinephrine, or 2mg/kg/day of dobutamine or 8mg/kg/day of salbutamol.

Western Blot Analysis

$CD45^+$ immune cells were isolated from CT2A tumor bearing mouse brains. Single cell suspensions were made, and cells were counted on a hemocytometer. $CD45^+$ immune cells were then isolated using CD45 positive selection kit (Stem Cell, cat# 100-0350) according to the manufacturer's instructions. Isolated immune cells were washed with PBS and spun down at 400g for 5 minutes. Cell pellet was placed on ice and resuspended in 200μL of lysis buffer. Lysis buffer was made as following: 10x lysis buffer (Cell Signaling, cat# 9803S) was diluted in ddH2O supplemented with 1mM PMSF (200x stock solution was purchased and reconstituted with 1ml of isopropanol-Cell Signaling, cat# 8553S), and 1x protease Protease/Phosphatase

Inhibitor Cocktail (100X stock solution cat# 5872S). Samples were incubated on ice for 5min and then rapidly sonicated in an ice bath sonicator. Samples were then spun at 14000g at 4C and the protein content of the supernatant was calculated using a BCA assay (Pierce, Cat # 23227). Samples were frozen at -20 C until the day assay was performed. Samples were diluted in 2x Laemmli Sample Buffer (Biorad, cat #1610737) supplemented with 2-Mercaptoethanol (Biorad, cat# 1610710 2-Mercaptoethanol). 950μL of 2x Laemmli buffer was mixed with 50μL of 2-Mercaptoethanol to obtain 2x sample buffer. Samples were loaded based on protein concentration and adjusted with lysis buffer supplemented with PMFS and protease/phosphatase inhibitor. Samples were then mixed with the 2x sample buffer in a 1:1 ratio. Samples were boiled at 95 C for 10min, and immediately cooled on ice for 5 mins before being loaded into a 4-20% gradient gel (Invitrogen, cat #XP04205BOX). Gel electrophoresis was performed at 100 constant volts until samples reached the bottom. Precision Plus Protein™ Kaleidoscope™ Prestained Protein Standards was used as a ladder (Biorad #1610375). PVDF membrane (Biorad, cat# 1620177) was activated in 100% methanol for 1min, then placed in ddH2O for 1min, and rested in 1x transfer buffer with 20% methanol (10x transfer buffer Cell Signaling, 12539S). 1x transfer buffer contained 100ml of 10x transfer buffer, 700ml of ddH2O, and 200ml of methanol. An overnight wet tank transfer was performed using 1x transfer buffer with 20% methanol using Mini Trans-Blot® Cell wet tank transfer system (Biorad, cat# 1703930) at 25 constant volts. Membrane was blocked with SuperBlock (Thermofisher, cat# 37515) for 90-120 minutes at 4°C on a shaker. Membranes were then cut and incubated with primary antibody and incubated overnight in 10mL of a mixture of SuperBlock and 1XTBST plus 10μL of primary antibody. The p65 antibody was from the NF-κB Pathway Antibody Sampler Kit (Cell Signaling, cat #9936). Antibodies against Histone H3 were used as loading control (Cell Signaling, cat # 4499S). Membranes were washed 5 times with 1x TBST (Cell Signaling, cat # 9997S) with gentle agitation on a shaker at room temperature. Membranes were then incubated with a mix of anti-rabbit and anti-mouse HRP conjugated secondary antibodies according to the instructions provided with NF-κB Pathway Antibody Sampler Kit in a mix of Superblock and 1x TBST for 60-90min on a shaker at room temperature. Membranes were washed 4 times in 1xTBST and once in 1x TBS (Cell Signaling, cat# 12498S) on a shaker at room temp. Membranes were developed using SuperSignal™ West Pico PLUS Chemiluminescent Substrate (Thermofihser, cat# 34580). Images were acquired and quantified on a Licor Odyssey FC running Image Studios software.

In vivo Imaging for Tumor Growth

Mice were implanted with 50K CT2A-Luciferase, ear-tagged such that individual mice could be followed, and imaged twice weekly, starting at day 10 after tumor implantation. Luciferin was resuspended at 15mg/mL. Mice were weighed then injected with a 150mg/kg luciferin, in groups of 2-3 mice at a time. Five minutes after luciferin injection, all mice were anesthetized in an isoflurane chamber. After an additional 2min, mice were transferred into the In Vivo Imaging System (IVIS) for imaging. Images were analyzed upon termination of the experiment where total flux (radiance) was measured for all mice across timepoints after images were adjusted to reflect the same scale on every image.

Flow Cytometry

Cells were first washed with PBS then resuspended in Zombie Aqua Viability Dye (1:500 in PBS, Biolegend). For extracellular staining, samples were first resuspended in 50μL TruStain FcX Plus (1:500, Biolegend) in FACS buffer (2% FBS in PBS) for 15min at room temperature to block Fc receptors. After blocking, 50μL of a 2x antibody mastermix was added to samples and samples were incubated for 30min at 4°C. Samples were then washed in FACs buffer and fixed

with 2% formaldehyde in PBS for 20min at 4°C or fix/permeabilized for subsequent intracellular staining.

For intracellular staining, samples were fixed and permeabilized with a 1X FoxP3 Fixation/Permeabilization Buffer (eBioscience FoxP3/Transcription Factor Staining Buffer Set, Thermo Fisher Scientific) for 30min at 4°C.

Prior to sample acquisition, 10μL of Count Bright counting beads (Thermo Fisher Scientific) in 40μL of FACs buffer were added to each sample. Samples were acquired on a Fortessa (BD Biosciences) using FACS Diva software v.9 and analyzed using FlowJo v.10 (Tree Star).

Information regarding antibodies can be found below:

Marker	Color	Company	Catalog #	Clone
Live/Dead	BV510	Biolegend	423102	NA (Dye)
CD45	APC-Cy7	Biolegend	103116	30-F11
CD3	PE-Cy5	Biolegend	100310	145-2C11
CD19	PE-Cy5	Biolegend	115509	6D5
NK1.1	PE-Cy5	Biolegend	108715	PK136
Ly6G	PE-Cy5	Invitrogen	15-9668-82	1A8-Ly6g
CD64	BV711	Biolegend	139311	X54-5/7.1
CD11c	BV786	Biolegend	117335	N418
CD11b	PE	Biolegend	101207	M1/70
Siglec-H	PE-Cy7	Invitrogen	25-0333-80	eBio440c
MHCII	AF488	Biolegend	107615	M5/114.15.2
CD8	BV650	Biolegend	100742	53-6.7
CD103	PE-Dazzle	Biolegend	121429	2E7
XCR1	BV421	Biolegend	148216	ZET
CD40	BV605	BD Biosciences	745218	23-Mar
CD86	APC	Biolegend	105011	GL-1
CD3	PE	BD Biosciences	553064	145-2C11
CD4	BV605	Biolegend	100548	RM4-5
CD8	APCR700	BD Biosciences	564983	53-6.7
CD11b	PE Dazzle	BD Biosciences	562287	M1/70
Ly6C	BV650	Biolegend	128049	HK1.4
Ly6G	BV421	Biolegend	127627	1A8
F4/80	PE-Cy5	Biolegend	123112	BM8

MHCII	AF488	Biolegend	107615	M5/114.15.2
FoxP3	PE-Cy5.5	Biolegend	320012	150D
CD44	BV786	Biolegend	103059	N418
PD1	PE-Dazzle	Biolegend	109116	RMP1-30
CD25	BV421	Biolegend	102043	PC61
CD40L	PE-Cy7	Biolegend	106512	MR1
CD62L	PE-Cy5	Biolegend	104410	MEL-14
KLRG1	APC	Biolegend	138412	2F1/KLRG1
CD69	BV711	Biolegend	104537	H1.2F3
FoxP3	AF488	Biolegend	320012	150D
CD8	BUV737	BD Biosciences	612759	53-6.7
iNOS	PE-Cy5.5	Invitrogen	35-5920-80	CXNFT
CD68	PE-Cy7	Biolegend	137015	FA-11
F4/80	PE-Cy5	Invitrogen	15-4801-82	BM8
CD206	PE-Dazzle 594	Biolegend	141731	C068C2
Arg1	PE	Invitrogen	12-3697-80	A1exF5
CD4	APC-Cy7	Biolegend	100526	RM4-5
CD11c	APCR700	BD Biosciences	565872	N418
TOX	EF600	Invitrogen	50-6502-82	TXRX10
MHCII	AF488	Biolegend	107616	M5/114.15.2
PDL1	BV785	Biolegend	124331	10F.9G2
CD19	BV750	Biolegend	115561	6D5
PD1	BV711	Biolegend	135231	29F.1A12
TIM3	BV421	Biolegend	119723	RMT3-23
SLAMF6	BV650	BD Biosciences	740628	13G3
Ly6G	BV605	BD Biosciences	563005	1A8
Ki67	BUV805	Invitrogen	368-5698-82	SolA15
CD11b	BV480	Invitrogen	414-0112-82	M1/70
CD3	BUV395	BD Biosciences	563565	14-2C11
CD45	BUV496	Invitrogen	364-0451-82	30-F11
Ly6C	BUV563	BD Biosciences	755198	HK1.4.rMab

CD44	BUV615	Invitrogen	366-0441-82	IM7

Single-Cell Cytokine Analysis

Spleens were harvested and T cells were isolated via untouched $CD8^+$ T cell isolation or Pan T cell isolation kits (Miltenyi) and stimulated ex vivo with plate-coated anti-CD3, soluble anti-CD28 antibodies (Invitrogen) for 16hours. T cells were then harvested and loaded into single-cell adaptive immune chips according to manufacturer instructions. Chips were run on the Isolight machine (Isoplexis) overnight and data were analyzed using IsoSpeak software (Isoplexis).

Immunofluorescence Imaging

Paraffin-embedded sample blocks of murine CT2A were utilized to prepare 5μm tissue sections on glass slides. One slide per sample was stained with a b2-adrenergic receptor (Abcam) primary antibody at 1:500 concentration. Slides were also stained with DAPI (1:20). One slide per sample was stained using non-immune rabbit and rat IgG (Invitrogen). Immunofluorescence was measured using a Leica SP5 inverted confocal microscope. Adrenergic receptor and nucleus expression were quantified using Qupath computer software. β2-adrenergic receptor expression was normalized to IgG control and DAPI expression.

Gene Expression Analysis

C57BL/6 mice were implanted with intracranial CT2A glioma and treated with propranolol or vehicle control as described above. An additional non-tumor bearing group was included. Tumors were harvested and combined (n=5 tumors per group) with n=3 biological replicates per sample for a total of 15 tumors per sample. Immune cells were FACS-sorted for APC-enriched samples or T cell-enriched samples and RNA was subsequently extracted (RNeasy Mini Kit, Qiagen). RNA was analyzed on an nCounter MAX Analysis System (Nanostring) with the PanCancer Immune Profiling panel (Nanostring) according to manufacturer instructions. Expression data were analyzed using Rosalind, nSolver and nSolver Advanced Analysis software.

Human Retrospective Data

SEER is a population-based cancer registry that collects data on newly diagnosed cancers and provides cancer statistics for these cancers. SEER data are aggregated from cancer registries and contain patient demographic and tumor characteristics as well as the first course of treatment. SEER-Medicare[135,136] is the result of a linkage between existing SEER case data and detailed information about Medicare beneficiary's covered healthcare services from the time of Medicare eligibility until death. Importantly, this database only includes individuals who are eligible for Medicare, which, in the U.S., generally occurs at age 65. Individuals may be eligible for Medicare at younger ages due to reasons such as disability or certain medical conditions, but these individuals were excluded from this analysis due to the potentially confounding effects of their qualifying conditions (ie. kidney failure necessitating dialysis). The linked dataset includes 15 SEER registries covering ~24% of the US population. Medicare included approximately 95% of patients age 65 and older in the SEER files[136]. Additionally, among all Medicare enrollees, the proportion of those enrolled in Medicare Advantage plans has increased from 21% in 2008 to 34% in 2018.[137] As enrollees in Advantage plans will lack claims for the time period they are enrolled, this restriction represents a significant limitation to the population that is able to be used. Furthermore, as some patients may have private health insurance or not be continuously enrolled in Medicare Part B in addition to Part A, there is a possibility that some

included individuals may have an incomplete claims history. Individuals were identified in the SEER cancer files for diagnoses made from January 1, 2008 – December 1, 2017, excluding patients younger than 65 years and those enrolled due to end-stage renal disease or disability **(ICD codes in Supplementary Table 1**). Patients enrolled in a Health Maintenance Organization six months prior and twelve months after primary diagnosis were excluded (34.1% of lung cancer, 31.3% of melanoma, 24.3% of GBM). Individuals with missing age, race, ethnicity, sex, and survival or follow-up time were excluded from the analysis. These exclusions were made to assure completeness of claims data in the analytic dataset.

Cases of primary GBM (International Classification of Diseases for Oncology 3rd Edition (ICD-O-3)[138] morphology codes 9440/3, 9441/3, 9442/3, 9445/3; topographic codes C71.0-C71.9), melanoma (ICD-O-3 morphology codes 8720/3-8790/3, ICD-O-3 topographic codes C44.0-C44.9) and lung cancer (ICD-O-3 morphology codes 8000/3-8579/3, ICD-O-3 topographic codes C34.0-C34.9) were identified in the SEER cancer file . Those with a prior cancer diagnosis, which was identified using a SEER-provided variable (*Sequence_number)*, were also excluded (36.9% of lung cancer, 53.9% of melanoma, 32.8% of GBM).

Intracranial metastases were identified using the SEER synchronous brain metastasis variable and the Medicare Provider Analysis and Review (MEDPAR), National Claims History (NCH), and Outpatient (OUTPAT) claims files as previously described in Ascha, et al.[127] Briefly, patients. Patients with intracranial metastases were defined as those with a diagnosis code for an intracranial metastasis (International Classification of Diseases 9th and 10th Ed. (ICD-9 and ICD-10) codes 198.3 and C79.3, respectively) and at least one procedure code for a brain or head diagnostic test within 60 days of the intracranial metastasis diagnosis (Current Procedural Terminology[139] codes 70450-70470, 70551-70553, 78607-78608). Prior comorbidity score was estimated using the rule-out option of the SEER-Medicare SAS comorbidity macro (2021 version)[140] using both ICD-9 and ICD-10 diagnosis codes. The comorbidity scores were calculated with Charlson weights and grouped as a score of 0, 1, 2, and 3+. Cancer treatment patterns – including radiation, chemotherapy, β-blocker, and checkpoint blockade usage (including Pembrolizumab, Necitumumab, Nivolumab, Ipilimumab, Atezolizumab, and Ramucirumab) – were identified using both SEER data and the MEDPAR, NCH, OUTPAT, Part D Event, and Durable Medical Equipment files. Surgery was identified using SEER -provided variable (*RX_Summ_Surg_prim-Site_1998)* which includes biopsies with excision and claims with CPT and ICD codes specific to the type of primary cancer (**Supplementary Table 1**). Radiation therapy and chemotherapy were defined by ≥2 claims for the same code separated by at least one week, and prior use of β-blockers was defined as ≥2 dispensing for the same β-blocker prior to diagnosis (**Supplementary Table 1**). Patients that started checkpoint blockade before detection of intracranial metastasis were excluded from the analysis.

Cases of lung and melanoma that have been determined to have brain metastases include those that are synchronous (found at initial diagnosis) and asynchronous (those found more than 1 month after diagnosis). Synchronous brain metastases were identified via a combination of the SEER-provided brain metastasis variables and a previously validated algorithm to detect brain metastases in claims data, while asynchronous brain metastases will be identified solely through the latter. Patients with asynchronous brain metastases may not be identified as stage IV at the initial diagnosis of their primary due to the follow-up information available through Medicare claims. Cases with extracranial metastases at diagnosis were identified using the SEER-provided stage at diagnosis variable only and did not include cases identified as having brain metastasis.

Sensitivity analyses showing the effects of concomitant β-blocker and checkpoint blockade in patients with lung cancer and melanoma that were identified as having continuous enrollment in Medicare Part A and B, as well as equivalent months of enrollment in Medicare Part D, showed no substantial differences in effect size from the unrestricted cohort.

Statistical Analyses

Experimental group assignment was determined by random designation. All measurements were taken from distinct samples. The statistical tests employed for each data presentation and number of samples (n) are designated in the respective figure legends. Individual data points are represented as dots in graphs. Statistical analyses were performed using GraphPad Prism software. Error bars represent the standard error of the mean (SEM). No data were excluded from analysis. Mice were randomized into treatment groups after tumor injection. P-values <0.05 were considered statistically significant. Investigators were not blinded to group assignment during experimental procedures or analysis, but survival studies were monitored both by investigators and additionally monitored by veterinary staff from the Duke animal facility who were blinded to the studies and reported humane endpoints accordingly.

Analyses of clinical data were performed stratified by cancer type within selected treatment groups. Kaplan-Meier estimation was used to assess the effect of a combination β-blocker and checkpoint blockade versus checkpoint blockade alone on overall survival. In GBM, where no checkpoint inhibitors are currently approved for use, the effect of β-blockers on overall survival was examined. Multivariable Cox proportional hazards models were used to assess the relationship between combination β-blocker and checkpoint blockade versus checkpoint blockade alone among the cohorts, adjusting for SEER-provided demographics and potential confounders, including age; sex (male or female); and race/ethnicity (non-Hispanic White, non-Hispanic Black, non-Hispanic Other, or Hispanic [all races], or Unknown); treatment pattern (yes/no surgery of primary tumor, radiation and chemotherapy); and prior comorbidity score. Sensitivity analyses were performed in the subset of individuals identified as having continuous enrollment in Medicare Part A and B, as well as equivalent months of enrollment in Medicare Part D as Medicare Part A and B. P-values <0.05 were considered statistically significant. All analyses of clinical data were conducted using R version 4.1.3 using the following packages: gtsummary, patchwork, survival, survminer, and tidyverse suite.[141-145]

Ethics statement

All studies performed in research animals and on clinical samples are compliant with all relevant ethical regulations. All animal experiments were approved by the IACUC at Duke University Medical Center (protocol A163-21-08). De-identified human samples were used in this study with exempt Institutional Review Board (IRB) status granted from the Duke University Health System Institutional Review Board (protocol ID: Pro00112766).

DATA AVAILABILITY

All scRNAseq datasets used for analysis are publicly available: GSE182109[129], GSE154795[130], GSE160189[131], GSE200218[132], and GSE186344[133]. SEER-Medicare data are publicly available, but these data are released on a project-specific basis that requires an approved application. Applications are reviewed by NCI-led content experts and application revisions may be required. Initial reviewer comments are typically provided within 2-3 weeks. Fees are incurred to cover the cost of creating the requested data files. Instructions for the application can be found here: https://healthcaredelivery.cancer.gov/seermedicare/obtain/requests.html#docs.
Gene expression data that support the findings of this study have been deposited in the Gene Expression Omnibus under the accession number GSE241720.

CODE AVAILABILITY

Integration and analysis of publicly available scRNAseq datasets were conducted based on publicly available workflows and can be accessed at https://github.com/jbfinlay/Lorrey_Wachsmuth_et_al. Analysis of relevant SEER-Medicare data can be accessed at https://zenodo.org/record/8289570.

REFERENCES

1 Reardon, D. A. *et al.* Effect of Nivolumab vs Bevacizumab in Patients With Recurrent Glioblastoma: The CheckMate 143 Phase 3 Randomized Clinical Trial. *JAMA Oncol* **6**, 1003-1010, doi:10.1001/jamaoncol.2020.1024 (2020).

2 Lim, M. *et al.* Phase III trial of chemoradiotherapy with temozolomide plus nivolumab or placebo for newly diagnosed glioblastoma with methylated MGMT promoter. *Neuro Oncol* **24**, 1935-1949, doi:10.1093/neuonc/noac116 (2022).

3 Omuro, A. *et al.* Radiotherapy combined with nivolumab or temozolomide for newly diagnosed glioblastoma with unmethylated MGMT promoter: An international randomized phase III trial. *Neuro Oncol* **25**, 123-134, doi:10.1093/neuonc/noac099 (2023).

4 Woroniecka, K. I., Rhodin, K. E., Chongsathidkiet, P., Keith, K. A. & Fecci, P. E. T-cell Dysfunction in Glioblastoma: Applying a New Framework. *Clin Cancer Res* **24**, 3792-3802, doi:10.1158/1078-0432.ccr-18-0047 (2018).

5 Brooks, W. H., Caldwell, H. D. & Mortara, R. H. Immune responses in patients with gliomas. *Surg Neurol* **2**, 419-423 (1974).

6 Brooks, W. H., Netsky, M. G., Normansell, D. E. & Horwitz, D. A. Depressed cell-mediated immunity in patients with primary intracranial tumors. Characterization of a humoral immunosuppressive factor. *J Exp Med* **136**, 1631-1647 (1972).

7 Brooks, W. H., Roszman, T. L., Mahaley, M. S. & Woosley, R. E. Immunobiology of primary intracranial tumours. II. Analysis of lymphocyte subpopulations in patients with primary brain tumours. *Clin Exp Immunol* **29**, 61-66 (1977).

8 Brooks, W. H., Roszman, T. L. & Rogers, A. S. Impairment of rosette-forming T lymphoctyes in patients with primary intracranial tumors. *Cancer* **37**, 1869-1873 (1976).

9 Dix, A. R., Brooks, W. H., Roszman, T. L. & Morford, L. A. Immune defects observed in patients with primary malignant brain tumors. *J Neuroimmunol* **100**, 216-232 (1999).

10 Elliott, L., Brooks, W. & Roszman, T. Role of interleukin-2 (IL-2) and IL-2 receptor expression in the proliferative defect observed in mitogen-stimulated lymphocytes from patients with gliomas. *Journal of the National Cancer Institute* **78**, 919-922 (1987).

11 Elliott, L. H., Brooks, W. H. & Roszman, T. L. Cytokinetic basis for the impaired activation of lymphocytes from patients with primary intracranial tumors. *Journal of Immunology* **132**, 1208-1215 (1984).

12 Elliott, L. H., Brooks, W. H. & Roszman, T. L. Inability of mitogen-activated lymphocytes obtained from patients with malignant primary intracranial tumors to express high affinity interleukin 2 receptors. *Journal of Clinical Investigation* **86**, 80-86 (1990).

13 Mahaley, M. S., Jr. *et al.* Immunobiology of primary intracranial tumors. Part 1: studies of the cellular and humoral general immune competence of brain-tumor patients. *Journal of Neurosurgery* **46**, 467-476 (1977).

14 McVicar, D. W., Davis, D. F. & Merchant, R. E. In vitro analysis of the proliferative potential of T cells from patients with brain tumor: glioma-associated immunosuppression unrelated to intrinsic cellular defect. *Journal of Neurosurgery* **76**, 251-260 (1992).

15 Morford, L. A., Elliott, L. H., Carlson, S. L., Brooks, W. H. & Roszman, T. L. T cell receptor-mediated signaling is defective in T cells obtained from patients with primary intracranial tumors. *Journal of Immunology* **159**, 4415-4425 (1997).

16 Roszman, T. L. & Brooks, W. H. Immunobiology of primary intracranial tumours. III. Demonstration of a qualitative lymphocyte abnormality in patients with primary brain tumours. *Clin Exp Immunol* **39**, 395-402 (1980).

17 Roszman, T. L., Brooks, W. H. & Elliott, L. H. Immunobiology of primary intracranial tumors. VI. Suppressor cell function and lectin-binding lymphocyte subpopulations in patients with cerebral tumors. *Cancer* **50**, 1273-1279 (1982).

18 Roszman, T. L., Brooks, W. H. & Elliott, L. H. Inhibition of lymphocyte responsiveness by a glial tumor cell-derived suppressive factor. *Journal of Neurosurgery* **67**, 874-879 (1987).

19 Young, H. F., Sakalas, R. & Kaplan, A. M. Inhibition of cell-mediated immunity in patients with brain tumors. *Surg Neurol* **5**, 19-23 (1976).

20 Chongsathidkiet, P. *et al.* Sequestration of T cells in bone marrow in the setting of glioblastoma and other intracranial tumors. *Nat Med* **24**, 1459-1468, doi:10.1038/s41591-018-0135-2 (2018).

21 Dunn, G. P., Fecci, P. E. & Curry, W. T. Cancer immunoediting in malignant glioma. *Neurosurgery* **71**, 201-223 (2012).

22 Fecci, P. E., Heimberger, A. B. & Sampson, J. H. Immunotherapy for primary brain tumors: no longer a matter of privilege. *Clin Cancer Res* **20**, 5620-5629, doi:10.1158/1078-0432.CCR-14-0832 (2014).

23 Fecci, P. E. & Sampson, J. H. The current state of immunotherapy for gliomas: an eye toward the future. *J Neurosurg* **131**, 657-666, doi:10.3171/2019.5.JNS181762 (2019).

24 Grabowski, M. M. *et al.* Immune suppression in gliomas. *J Neurooncol* **151**, 3-12, doi:10.1007/s11060-020-03483-y (2021).

25 Miggelbrink, A. M. *et al.* CD4 T-Cell Exhaustion: Does It Exist and What Are Its Roles in Cancer? *Clin Cancer Res* **27**, 5742-5752, doi:10.1158/1078-0432.CCR-21-0206 (2021).

26 Sampson, J. H., Gunn, M. D., Fecci, P. E. & Ashley, D. M. Brain immunology and immunotherapy in brain tumours. *Nat Rev Cancer* **20**, 12-25, doi:10.1038/s41568-019-0224-7 (2020).

27 Woroniecka, K. *et al.* T Cell Exhaustion Signatures Vary with Tumor Type and are Severe in Glioblastoma. *Clin Cancer Res*, doi:10.1158/1078-0432.ccr-17-1846 (2018).

28 Fecci, P. E. *et al.* Systemic CTLA-4 blockade ameliorates glioma-induced changes to the CD4+ T cell compartment without affecting regulatory T-cell function. *Clin Cancer Res* **13**, 2158-2167, doi:13/7/2158 [pii]
10.1158/1078-0432.CCR-06-2070 (2007).

29 Kizaki, T. *et al.* Beta2-adrenergic receptor regulates Toll-like receptor-4-induced nuclear factor-kappaB activation through beta-arrestin 2. *Immunology* **124**, 348-356, doi:10.1111/j.1365-2567.2007.02781.x (2008).

30 Safi, S. Z. *et al.* Beta Adrenergic Receptors Stimulation Attenuates Phosphorylation of NF-kappaB and IkappaBalpha in Hyperglycemic Endothelial Cells. *Cell Physiol Biochem* **51**, 1429-1436, doi:10.1159/000495591 (2018).

31 Takenaka, M. C. *et al.* Norepinephrine Controls Effector T Cell Differentiation through beta2-Adrenergic Receptor-Mediated Inhibition of NF-kappaB and AP-1 in Dendritic Cells. *J Immunol* **196**, 637-644, doi:10.4049/jimmunol.1501206 (2016).

32 Farmer, P. & Pugin, J. beta-adrenergic agonists exert their "anti-inflammatory" effects in monocytic cells through the IkappaB/NF-kappaB pathway. *Am J Physiol Lung Cell Mol Physiol* **279**, L675-682, doi:10.1152/ajplung.2000.279.4.L675 (2000).
33 Verhoeckx, K. C., Doornbos, R. P., van der Greef, J., Witkamp, R. F. & Rodenburg, R. J. Inhibitory effects of the beta-adrenergic receptor agonist zilpaterol on the LPS-induced production of TNF-alpha in vitro and in vivo. *J Vet Pharmacol Ther* **28**, 531-537, doi:10.1111/j.1365-2885.2005.00691.x (2005).
34 Izeboud, C. A., Monshouwer, M., van Miert, A. S. & Witkamp, R. F. The beta-adrenoceptor agonist clenbuterol is a potent inhibitor of the LPS-induced production of TNF-alpha and IL-6 in vitro and in vivo. *Inflamm Res* **48**, 497-502, doi:10.1007/s000110050493 (1999).
35 Haddad, A. F. *et al.* Mouse models of glioblastoma for the evaluation of novel therapeutic strategies. *Neurooncol Adv* **3**, vdab100, doi:10.1093/noajnl/vdab100 (2021).
36 Ausiello, C. M. *et al.* Cell mediated cytotoxicity and cytokine production in peripheral blood mononuclear cells of glioma patients. *European Journal of Cancer* **27**, 646-650 (1991).
37 Dunn, G. P., Fecci, P. E. & Curry, W. T. Cancer immunoediting in malignant glioma. *Neurosurgery* **71**, 201-222; discussion 222-203, doi:10.1227/NEU.0b013e31824f840d (2012).
38 Morford, L. A., Dix, A. R., Brooks, W. H. & Roszman, T. L. Apoptotic elimination of peripheral T lymphocytes in patients with primary intracranial tumors. *Journal of Neurosurgery* **91**, 935-946 (1999).
39 Roussel, E., Gingras, M. C., Grimm, E. A., Bruner, J. M. & Moser, R. P. Predominance of a type 2 intratumoural immune response in fresh tumour-infiltrating lymphocytes from human gliomas. *Clin Exp Immunol* **105**, 344-352 (1996).
40 Young, H. F. & Kaplan, A. M. Cellular immune deficiency in patients with glioblastoma. *Surg Forum* **27**, 476-478 (1976).
41 Young, H. F., Sakalas, R. & Kaplan, A. M. Immunologic depression in cerebral gliomas. *Adv Neurol* **15**, 327-335 (1976).
42 Fecci, P. E. *et al.* Increased regulatory T-cell fraction amidst a diminished CD4 compartment explains cellular immune defects in patients with malignant glioma. *Cancer Res* **66**, 3294-3302, doi:10.1158/0008-5472.CAN-05-3773 (2006).
43 Reap, E. A. *et al.* Dendritic Cells Enhance Polyfunctionality of Adoptively Transferred T Cells That Target Cytomegalovirus in Glioblastoma. *Cancer Res* **78**, 256-264, doi:10.1158/0008-5472.can-17-0469 (2018).
44 Huff, W. X. *et al.* Aging- and Tumor-Mediated Increase in CD8(+)CD28(-) T Cells Might Impose a Strong Barrier to Success of Immunotherapy in Glioblastoma. *Immunohorizons* **5**, 395-409, doi:10.4049/immunohorizons.2100008 (2021).
45 Thibaudin, M. *et al.* Targeting PD-L1 and TIGIT could restore intratumoral CD8 T cell function in human colorectal cancer. *Cancer Immunol Immunother* **71**, 2549-2563, doi:10.1007/s00262-022-03182-9 (2022).
46 Miller, B. C. *et al.* Subsets of exhausted CD8(+) T cells differentially mediate tumor control and respond to checkpoint blockade. *Nat Immunol* **20**, 326-336, doi:10.1038/s41590-019-0312-6 (2019).
47 Ma, L. *et al.* Enhanced CAR-T cell activity against solid tumors by vaccine boosting through the chimeric receptor. *Science* **365**, 162-168, doi:10.1126/science.aav8692 (2019).
48 Sarkar, S. *et al.* Programming of CD8 T Cell Quantity and Polyfunctionality by Direct IL-1 Signals. *J Immunol* **201**, 3641-3650, doi:10.4049/jimmunol.1800906 (2018).

49 Zurko, J. C. *et al.* Bispecific targeting of CD20 and CD19 increases polyfunctionality of chimeric antigen receptor T-cell products in B-cell malignancies. *Cytotherapy* **24**, 767-773, doi:10.1016/j.jcyt.2022.03.011 (2022).
50 Yoshikawa, T. *et al.* Genetic ablation of PRDM1 in antitumor T cells enhances therapeutic efficacy of adoptive immunotherapy. *Blood* **139**, 2156-2172, doi:10.1182/blood.2021012714 (2022).
51 Sung, B. Y. *et al.* Wnt activation promotes memory T cell polyfunctionality via epigenetic regulator PRMT1. *J Clin Invest* **132**, doi:10.1172/JCI140508 (2022).
52 Doescher, J. *et al.* Polyfunctionality of CD4(+) T lymphocytes is increased after chemoradiotherapy of head and neck squamous cell carcinoma. *Strahlenther Onkol* **194**, 392-402, doi:10.1007/s00066-018-1289-z (2018).
53 Kaptein, P. *et al.* Addition of interleukin-2 overcomes resistance to neoadjuvant CTLA4 and PD1 blockade in ex vivo patient tumors. *Sci Transl Med* **14**, eabj9779, doi:10.1126/scitranslmed.abj9779 (2022).
54 Migueles, S. A. *et al.* Defective human immunodeficiency virus-specific CD8+ T-cell polyfunctionality, proliferation, and cytotoxicity are not restored by antiretroviral therapy. *J Virol* **83**, 11876-11889, doi:10.1128/JVI.01153-09 (2009).
55 Egelston, C. A. *et al.* Human breast tumor-infiltrating CD8(+) T cells retain polyfunctionality despite PD-1 expression. *Nat Commun* **9**, 4297, doi:10.1038/s41467-018-06653-9 (2018).
56 Ramello, M. C. *et al.* Polyfunctional KLRG-1(+)CD57(+) Senescent CD4(+) T Cells Infiltrate Tumors and Are Expanded in Peripheral Blood From Breast Cancer Patients. *Front Immunol* **12**, 713132, doi:10.3389/fimmu.2021.713132 (2021).
57 Rossi, J. *et al.* Preinfusion polyfunctional anti-CD19 chimeric antigen receptor T cells are associated with clinical outcomes in NHL. *Blood* **132**, 804-814, doi:10.1182/blood-2018-01-828343 (2018).
58 Globig, A. M. *et al.* The beta(1)-adrenergic receptor links sympathetic nerves to T cell exhaustion. *Nature* **622**, 383-392, doi:10.1038/s41586-023-06568-6 (2023).
59 Wang, H. *et al.* beta-arrestin2 functions as a key regulator in the sympathetic-triggered immunodepression after stroke. *J Neuroinflammation* **15**, 102, doi:10.1186/s12974-018-1142-4 (2018).
60 Giridharan, S. & Srinivasan, M. Mechanisms of NF-kappaB p65 and strategies for therapeutic manipulation. *J Inflamm Res* **11**, 407-419, doi:10.2147/JIR.S140188 (2018).
61 Liu, T., Zhang, L., Joo, D. & Sun, S. C. NF-kappaB signaling in inflammation. *Signal Transduct Target Ther* **2**, 17023-, doi:10.1038/sigtrans.2017.23 (2017).
62 Barnes, S. E. *et al.* T cell-NF-kappaB activation is required for tumor control in vivo. *J Immunother Cancer* **3**, 1, doi:10.1186/s40425-014-0045-x (2015).
63 Bottcher, J. P. & Reis e Sousa, C. The Role of Type 1 Conventional Dendritic Cells in Cancer Immunity. *Trends Cancer* **4**, 784-792, doi:10.1016/j.trecan.2018.09.001 (2018).
64 Cancel, J. C., Crozat, K., Dalod, M. & Mattiuz, R. Are Conventional Type 1 Dendritic Cells Critical for Protective Antitumor Immunity and How? *Front Immunol* **10**, 9, doi:10.3389/fimmu.2019.00009 (2019).
65 Marigo, I. *et al.* T Cell Cancer Therapy Requires CD40-CD40L Activation of Tumor Necrosis Factor and Inducible Nitric-Oxide-Synthase-Producing Dendritic Cells. *Cancer Cell* **30**, 651, doi:10.1016/j.ccell.2016.09.009 (2016).
66 Frentsch, M. *et al.* CD40L expression permits CD8+ T cells to execute immunologic helper functions. *Blood* **122**, 405-412, doi:10.1182/blood-2013-02-483586 (2013).
67 Watowich, M. B., Gilbert, M. R. & Larion, M. T cell exhaustion in malignant gliomas. *Trends Cancer* **9**, 270-292, doi:10.1016/j.trecan.2022.12.008 (2023).
68 Woroniecka, K. & Fecci, P. E. T-cell exhaustion in glioblastoma. *Oncotarget* **9**, 35287-35288, doi:10.18632/oncotarget.26228 (2018).

69 Woroniecka, K. I. *et al.* 4-1BB Agonism Averts TIL Exhaustion and Licenses PD-1 Blockade in Glioblastoma and Other Intracranial Cancers. *Clin Cancer Res* **26**, 1349-1358, doi:10.1158/1078-0432.CCR-19-1068 (2020).

70 Noffsinger, B. *et al.* Technical choices significantly alter the adaptive immune response against immunocompetent murine gliomas in a model-dependent manner. *J Neurooncol* **154**, 145-157, doi:10.1007/s11060-021-03822-7 (2021).

71 Batalla-Covello, J., Ali, S., Xie, T. & Amit, M. β-Adrenergic signaling in skin cancer. *FASEB Bioadv* **4**, 225-234, doi:10.1096/fba.2021-00097 (2022).

72 Gandhi, S. *et al.* Phase I Clinical Trial of Combination Propranolol and Pembrolizumab in Locally Advanced and Metastatic Melanoma: Safety, Tolerability, and Preliminary Evidence of Antitumor Activity. *Clin Cancer Res* **27**, 87-95, doi:10.1158/1078-0432.CCR-20-2381 (2021).

73 Kokolus, K. M. *et al.* Beta blocker use correlates with better overall survival in metastatic melanoma patients and improves the efficacy of immunotherapies in mice. *Oncoimmunology* **7**, e1405205, doi:10.1080/2162402X.2017.1405205 (2018).

74 Rains, S. L., Amaya, C. N. & Bryan, B. A. Beta-adrenergic receptors are expressed across diverse cancers. *Oncoscience* **4**, 95-105, doi:10.18632/oncoscience.357 (2017).

75 Powe, D. G. *et al.* Beta-blocker drug therapy reduces secondary cancer formation in breast cancer and improves cancer specific survival. *Oncotarget* **1**, 628-638, doi:10.18632/oncotarget.101009 (2010).

76 Wang, H. M. *et al.* Improved survival outcomes with the incidental use of beta-blockers among patients with non-small-cell lung cancer treated with definitive radiation therapy. *Annals of oncology : official journal of the European Society for Medical Oncology / ESMO* **24**, 1312-1319, doi:10.1093/annonc/mds616 (2013).

77 Watkins, J. L. *et al.* Clinical impact of selective and nonselective beta-blockers on survival in patients with ovarian cancer. *Cancer* **121**, 3444-3451, doi:10.1002/cncr.29392 (2015).

78 Kennedy, O. J. *et al.* Prognostic and predictive value of β-blockers in the EORTC 1325/KEYNOTE-054 phase III trial of pembrolizumab versus placebo in resected high-risk stage III melanoma. *Eur J Cancer* **165**, 97-112, doi:10.1016/j.ejca.2022.01.017 (2022).

79 Rui, Y. & Green, J. J. Overcoming delivery barriers in immunotherapy for glioblastoma. *Drug Deliv Transl Res* **11**, 2302-2316, doi:10.1007/s13346-021-01008-2 (2021).

80 Bechmann, I., Galea, I. & Perry, V. H. What is the blood-brain barrier (not)? *Trends Immunol* **28**, 5-11, doi:10.1016/j.it.2006.11.007 (2007).

81 Owens, T., Bechmann, I. & Engelhardt, B. Perivascular spaces and the two steps to neuroinflammation. *J Neuropathol Exp Neurol* **67**, 1113-1121, doi:10.1097/NEN.0b013e31818f9ca8 (2008).

82 Gajewski, T. F., Schreiber, H. & Fu, Y. X. Innate and adaptive immune cells in the tumor microenvironment. *Nat Immunol* **14**, 1014-1022, doi:10.1038/ni.2703 (2013).

83 Gajewski, T. F. *et al.* Cancer Immunotherapy Targets Based on Understanding the T Cell-Inflamed Versus Non-T Cell-Inflamed Tumor Microenvironment. *Adv Exp Med Biol* **1036**, 19-31, doi:10.1007/978-3-319-67577-0_2 (2017).

84 Quail, D. F. & Joyce, J. A. The Microenvironmental Landscape of Brain Tumors. *Cancer Cell* **31**, 326-341, doi:10.1016/j.ccell.2017.02.009 (2017).

85 Perng, P. & Lim, M. Immunosuppressive Mechanisms of Malignant Gliomas: Parallels at Non-CNS Sites. *Front Oncol* **5**, 153, doi:10.3389/fonc.2015.00153 (2015).

86 Bausart, M., Preat, V. & Malfanti, A. Immunotherapy for glioblastoma: the promise of combination strategies. *J Exp Clin Cancer Res* **41**, 35, doi:10.1186/s13046-022-02251-2 (2022).

87 Himes, B. T. *et al.* Immunosuppression in Glioblastoma: Current Understanding and Therapeutic Implications. *Front Oncol* **11**, 770561, doi:10.3389/fonc.2021.770561 (2021).

88 Dix, A. R., Brooks, W. H., Roszman, T. L. & Morford, L. A. Immune defects observed in patients with primary malignant brain tumors. *J Neuroimmunol* **100**, 216-232, doi:10.1016/s0165-5728(99)00203-9 (1999).

89 Lorrey, S. W. P., J.; Wachsmuth, LP.; Hoyt-Miggelbrink, A.; Tritz, Z.; Edwards, R.; Wolf, DM.; Johnson, AJ.; Fecci, PE.; Ayasoufi, K. Systemic immune derangements are shared across various CNS pathologies and reflect novel mechanisms of immune privilege. *Neuro-Oncology Advances*, doi: https://doi.org/10.1093/noajnl/vdad035 (2023).

90 Lorrey, S. J. *et al.* Systemic immune derangements are shared across various CNS pathologies and reflect novel mechanisms of immune privilege. *Neurooncol Adv* **5**, vdad035, doi:10.1093/noajnl/vdad035 (2023).

91 Bucsek, M. J., Giridharan, T., MacDonald, C. R., Hylander, B. L. & Repasky, E. A. An overview of the role of sympathetic regulation of immune responses in infectious disease and autoimmunity. *Int J Hyperthermia* **34**, 135-143, doi:10.1080/02656736.2017.1411621 (2018).

92 Devi, S. *et al.* Adrenergic regulation of the vasculature impairs leukocyte interstitial migration and suppresses immune responses. *Immunity* **54**, 1219-1230 e1217, doi:10.1016/j.immuni.2021.03.025 (2021).

93 Chen, M. *et al.* Adrenergic stress constrains the development of anti-tumor immunity and abscopal responses following local radiation. *Nat Commun* **11**, 1821, doi:10.1038/s41467-020-15676-0 (2020).

94 Balood, M. *et al.* Nociceptor neurons affect cancer immunosurveillance. *Nature* **611**, 405-412, doi:10.1038/s41586-022-05374-w (2022).

95 Westendorp, W. F., Nederkoorn, P. J., Vermeij, J. D., Dijkgraaf, M. G. & van de Beek, D. Post-stroke infection: a systematic review and meta-analysis. *BMC Neurol* **11**, 110, doi:10.1186/1471-2377-11-110 (2011).

96 Deng, Q. W. *et al.* Blocking Sympathetic Nervous System Reverses Partially Stroke-Induced Immunosuppression but does not Aggravate Functional Outcome After Experimental Stroke in Rats. *Neurochem Res* **41**, 1877-1886, doi:10.1007/s11064-016-1899-8 (2016).

97 Singh, A. & Ranjan, A. Adrenergic receptor signaling regulates the CD40-receptor mediated anti-tumor immunity. *Front Immunol* **14**, 1141712, doi:10.3389/fimmu.2023.1141712 (2023).

98 Zhu, J. *et al.* Tumour immune rejection triggered by activation of alpha2-adrenergic receptors. *Nature* **618**, 607-615, doi:10.1038/s41586-023-06110-8 (2023).

99 Mohammadpour, H., MacDonald, C. R., McCarthy, P. L., Abrams, S. I. & Repasky, E. A. beta2-adrenergic receptor signaling regulates metabolic pathways critical to myeloid-derived suppressor cell function within the TME. *Cell Rep* **37**, 109883, doi:10.1016/j.celrep.2021.109883 (2021).

100 Mohammadpour, H. *et al.* beta2 adrenergic receptor-mediated signaling regulates the immunosuppressive potential of myeloid-derived suppressor cells. *J Clin Invest* **129**, 5537-5552, doi:10.1172/JCI129502 (2019).

101 Fjaestad, K. Y. *et al.* Blockade of beta-adrenergic receptors reduces cancer growth and enhances the response to anti-CTLA4 therapy by modulating the tumor microenvironment. *Oncogene* **41**, 1364-1375, doi:10.1038/s41388-021-02170-0 (2022).

102 Calvani, M. *et al.* Norepinephrine promotes tumor microenvironment reactivity through beta3-adrenoreceptors during melanoma progression. *Oncotarget* **6**, 4615-4632, doi:10.18632/oncotarget.2652 (2015).

103 Eng, J. W. *et al.* A nervous tumor microenvironment: the impact of adrenergic stress on cancer cells, immunosuppression, and immunotherapeutic response. *Cancer Immunol Immunother* **63**, 1115-1128, doi:10.1007/s00262-014-1617-9 (2014).
104 De Giorgi, V. *et al.* Effect of beta-blockers and other antihypertensive drugs on the risk of melanoma recurrence and death. *Mayo Clin Proc* **88**, 1196-1203, doi:10.1016/j.mayocp.2013.09.001 (2013).
105 De Giorgi, V. *et al.* Propranolol for Off-label Treatment of Patients With Melanoma: Results From a Cohort Study. *JAMA Oncol* **4**, e172908, doi:10.1001/jamaoncol.2017.2908 (2018).
106 McCourt, C. *et al.* Beta-blocker usage after malignant melanoma diagnosis and survival: a population-based nested case-control study. *Br J Dermatol* **170**, 930-938, doi:10.1111/bjd.12894 (2014).
107 Katsarelias, D. *et al.* The Effect of Beta-Adrenergic Blocking Agents in Cutaneous Melanoma-A Nation-Wide Swedish Population-Based Retrospective Register Study. *Cancers (Basel)* **12**, doi:10.3390/cancers12113228 (2020).
108 Kim, H. S. *et al.* Propranolol Inhibits the Proliferation of Human Glioblastoma Cell Lines through Notch1 and Hes1 Signaling System. *J Korean Neurosurg Soc* **64**, 716-725, doi:10.3340/jkns.2021.0068 (2021).
109 Tewarie, I. A., Senders, J. T., Hulsbergen, A. F. C., Kremer, S. & Broekman, M. L. D. Beta-blockers and glioma: a systematic review of preclinical studies and clinical results. *Neurosurg Rev* **44**, 669-677, doi:10.1007/s10143-020-01277-4 (2021).
110 Prados, M. D. *et al.* Toward precision medicine in glioblastoma: the promise and the challenges. *Neuro Oncol* **17**, 1051-1063, doi:10.1093/neuonc/nov031 (2015).
111 Wang, X. *et al.* Norepinephrine promotes glioma cell migration through up-regulating the expression of Twist1. *BMC cancer* **22**, 213, doi:10.1186/s12885-022-09330-9 (2022).
112 Nissen, M. D., Sloan, E. K. & Mattarollo, S. R. beta-Adrenergic Signaling Impairs Antitumor CD8(+) T-cell Responses to B-cell Lymphoma Immunotherapy. *Cancer Immunol Res* **6**, 98-109, doi:10.1158/2326-6066.CIR-17-0401 (2018).
113 Qiao, G. *et al.* Chronic Adrenergic Stress Contributes to Metabolic Dysfunction and an Exhausted Phenotype in T Cells in the Tumor Microenvironment. *Cancer Immunol Res* **9**, 651-664, doi:10.1158/2326-6066.CIR-20-0445 (2021).
114 Bucsek, M. J. *et al.* beta-Adrenergic Signaling in Mice Housed at Standard Temperatures Suppresses an Effector Phenotype in CD8(+) T Cells and Undermines Checkpoint Inhibitor Therapy. *Cancer Res* **77**, 5639-5651, doi:10.1158/0008-5472.CAN-17-0546 (2017).
115 Daher, C. *et al.* Blockade of beta-Adrenergic Receptors Improves CD8(+) T-cell Priming and Cancer Vaccine Efficacy. *Cancer Immunol Res* **7**, 1849-1863, doi:10.1158/2326-6066.CIR-18-0833 (2019).
116 Ostrom, Q. T., Wright, C. H. & Barnholtz-Sloan, J. S. Brain metastases: epidemiology. *Handb Clin Neurol* **149**, 27-42, doi:10.1016/B978-0-12-811161-1.00002-5 (2018).
117 Barnholtz-Sloan, J. S. *et al.* Incidence proportions of brain metastases in patients diagnosed (1973 to 2001) in the Metropolitan Detroit Cancer Surveillance System. *J Clin Oncol* **22**, 2865-2872, doi:10.1200/JCO.2004.12.149 (2004).
118 Wrobel, L. J., Gayet-Ageron, A. & Le Gal, F. A. Effects of Beta-Blockers on Melanoma Microenvironment and Disease Survival in Human. *Cancers (Basel)* **12**, doi:10.3390/cancers12051094 (2020).
119 Jean Wrobel, L. *et al.* Propranolol induces a favourable shift of anti-tumor immunity in a murine spontaneous model of melanoma. *Oncotarget* **7**, 77825-77837, doi:10.18632/oncotarget.12833 (2016).

120 Ashrafi, S., Shapouri, R., Shirkhani, A. & Mahdavi, M. Anti-tumor effects of propranolol: Adjuvant activity on a transplanted murine breast cancer model. *Biomed Pharmacother* **104**, 45-51, doi:10.1016/j.biopha.2018.05.002 (2018).
121 Johansen, M. D. *et al.* Outcome of Bevacizumab Therapy in Patients with Recurrent Glioblastoma Treated with Angiotensin System Inhibitors. *Cancer Invest* **36**, 512-519, doi:10.1080/07357907.2018.1544639 (2018).
122 Nordstrom, B. L., Whyte, J. L., Stolar, M., Mercaldi, C. & Kallich, J. D. Identification of metastatic cancer in claims data. *Pharmacoepidemiology and Drug Safety* **21**, 21-28, doi:https://doi.org/10.1002/pds.3247 (2012).
123 Motheral, B. R. & Fairman, K. A. The use of claims databases for outcomes research: rationale, challenges, and strategies. *Clinical Therapeutics* **19**, 346-366, doi:https://doi.org/10.1016/S0149-2918(97)80122-1 (1997).
124 Strom, B. L. & Carson, J. L. Use of automated databases for pharmacoepidemiology research. *Epidemiol Rev* **12**, 87-107, doi:10.1093/oxfordjournals.epirev.a036064 (1990).
125 Jollis, J. G. *et al.* Discordance of databases designed for claims payment versus clinical information systems. Implications for outcomes research. *Ann Intern Med* **119**, 844-850, doi:10.7326/0003-4819-119-8-199310150-00011 (1993).
126 Strom, B. L. Data validity issues in using claims data. *Pharmacoepidemiol Drug Saf* **10**, 389-392, doi:10.1002/pds.610 (2001).
127 Ascha, M. S. *et al.* Lifetime Occurrence of Brain Metastases Arising from Lung, Breast, and Skin Cancers in the Elderly: A SEER-Medicare Study. *Cancer Epidemiol Biomarkers Prev* **28**, 917-925, doi:10.1158/1055-9965.Epi-18-1116 (2019).
128 Srinivasan, A. V. Propranolol: A 50-Year Historical Perspective. *Ann Indian Acad Neurol* **22**, 21-26, doi:10.4103/aian.AIAN_201_18 (2019).
129 Abdelfattah, N. *et al.* Single-cell analysis of human glioma and immune cells identifies S100A4 as an immunotherapy target. *Nat Commun* **13**, 767, doi:10.1038/s41467-022-28372-y (2022).
130 Lee, A. H. *et al.* Neoadjuvant PD-1 blockade induces T cell and cDC1 activation but fails to overcome the immunosuppressive tumor associated macrophages in recurrent glioblastoma. *Nat Commun* **12**, 6938, doi:10.1038/s41467-021-26940-2 (2021).
131 Ayhan, F. *et al.* Resolving cellular and molecular diversity along the hippocampal anterior-to-posterior axis in humans. *Neuron* **109**, 2091-2105 e2096, doi:10.1016/j.neuron.2021.05.003 (2021).
132 Biermann, J. *et al.* Dissecting the treatment-naive ecosystem of human melanoma brain metastasis. *Cell* **185**, 2591-2608 e2530, doi:10.1016/j.cell.2022.06.007 (2022).
133 Gonzalez, H. *et al.* Cellular architecture of human brain metastases. *Cell* **185**, 729-745 e720, doi:10.1016/j.cell.2021.12.043 (2022).
134 Heumos, L. *et al.* Best practices for single-cell analysis across modalities. *Nat Rev Genet* **24**, 550-572, doi:10.1038/s41576-023-00586-w (2023).
135 Enewold, L. *et al.* Updated Overview of the SEER-Medicare Data: Enhanced Content and Applications. *J Natl Cancer Inst Monogr* **2020**, 3-13, doi:10.1093/jncimonographs/lgz029 (2020).
136 (ed National Cancer Institute) (2022).
137 Neuman, P. & Jacobson, G. A. Medicare Advantage Checkup. *New England Journal of Medicine* **379**, 2163-2172, doi:10.1056/NEJMhpr1804089 (2018).
138 Fritz A, P. C., Jack A, Shanmugaratnam K, Sobin L, Perkin DM, Whelan S (World Health Organization, 2000).
139 Dotson, P. CPT(®) Codes: What Are They, Why Are They Necessary, and How Are They Developed? *Adv Wound Care (New Rochelle)* **2**, 583-587, doi:10.1089/wound.2013.0483 (2013).

140 Program, H. D. R. *Comorbidity SAS Macro (2021 version)*, <https://healthcaredelivery.cancer.gov/seermedicare/considerations/macro-2021.html> (2021).
141 Daniel D. Sjoberg, K. W., Michael Curry, Jessica A. Lavery and Joseph Larmarange. Reproducible Summary Tables with the gtsummary Package. *The R Journal* **13**, 570-580 (2021).
142 Thomas Lin Pedersen v. R package version 1.1.1 (2020).
143 Terry M. Therneau, P. M. G. *A Package for Survival Analysis in R.* R package version 3.2-11 edn, (2021).
144 survminer: Drawing Survival Curves using 'ggplot2'. v. R package version 0.4.9. (2021).
145 Wickham, H. A., M; Bryan, J et al. . Welcome to the tidyverse. *Journal of Open Source Software* **4**, 1686, doi:https://doi.org/10.21105/joss.01686 (2019).

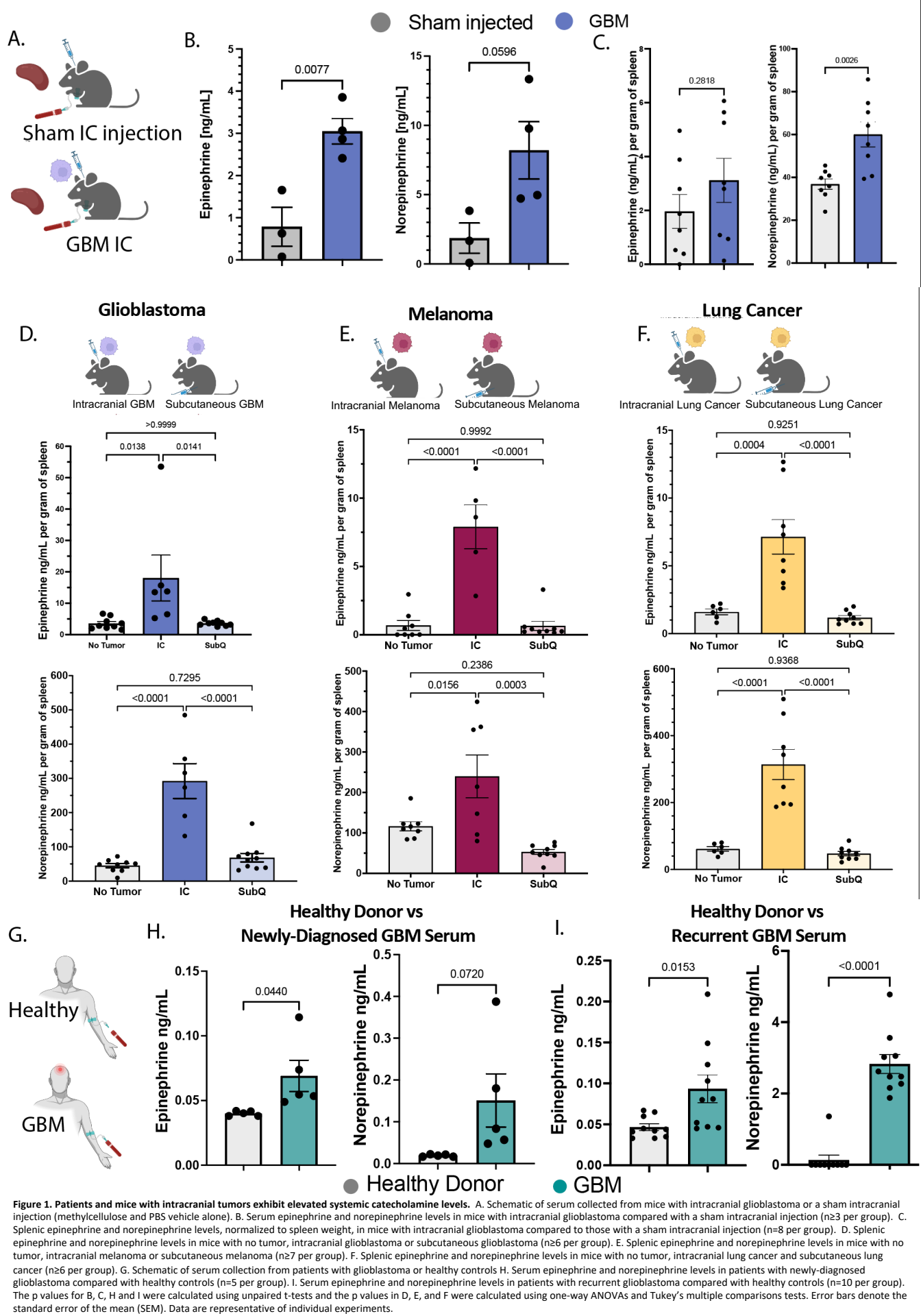

Figure 1. Patients and mice with intracranial tumors exhibit elevated systemic catecholamine levels. A. Schematic of serum collected from mice with intracranial glioblastoma or a sham intracranial injection (methylcellulose and PBS vehicle alone). B. Serum epinephrine and norepinephrine levels in mice with intracranial glioblastoma compared with a sham intracranial injection (n≥3 per group). C. Splenic epinephrine and norepinephrine levels, normalized to spleen weight, in mice with intracranial glioblastoma compared to those with a sham intracranial injection (n=8 per group). D. Splenic epinephrine and norepinephrine levels in mice with no tumor, intracranial glioblastoma or subcutaneous glioblastoma (n≥6 per group). E. Splenic epinephrine and norepinephrine levels in mice with no tumor, intracranial melanoma or subcutaneous melanoma (n≥7 per group). F. Splenic epinephrine and norepinephrine levels in mice with no tumor, intracranial lung cancer and subcutaneous lung cancer (n≥6 per group). G. Schematic of serum collection from patients with glioblastoma or healthy controls H. Serum epinephrine and norepinephrine levels in patients with newly-diagnosed glioblastoma compared with healthy controls (n=5 per group). I. Serum epinephrine and norepinephrine levels in patients with recurrent glioblastoma compared with healthy controls (n=10 per group). The p values for B, C, H and I were calculated using unpaired t-tests and the p values in D, E, and F were calculated using one-way ANOVAs and Tukey's multiple comparisons tests. Error bars denote the standard error of the mean (SEM). Data are representative of individual experiments.

A

GEO Accession	Tissue type
GSE182109	2 low grade glioma 10 newly diagnosed GBM 5 recurrent GBM
GSE154795	14 newly diagnosed GBM 12 recurrent GBM 5 PBMCs from recurrent GBM patients 2 healthy donor PBMCs
GSE160189	5 normal brain
GSE200218	5 melanoma brain metastases
GSE186344	3 breast cancer brain metastases 3 lung cancer brain metastases 3 melanoma brain metastases

Total: 69 patients (552,442 cells)

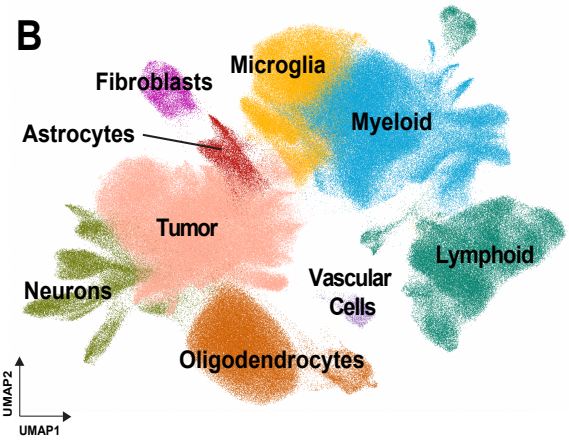

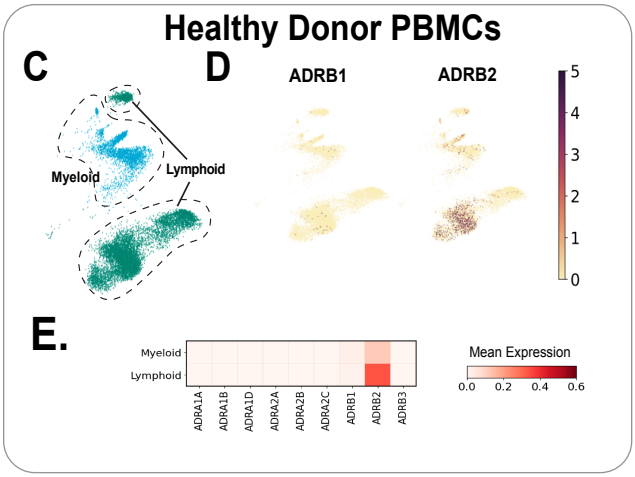

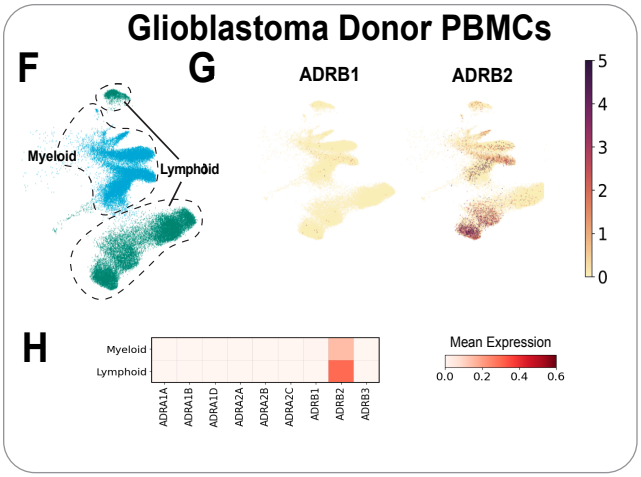

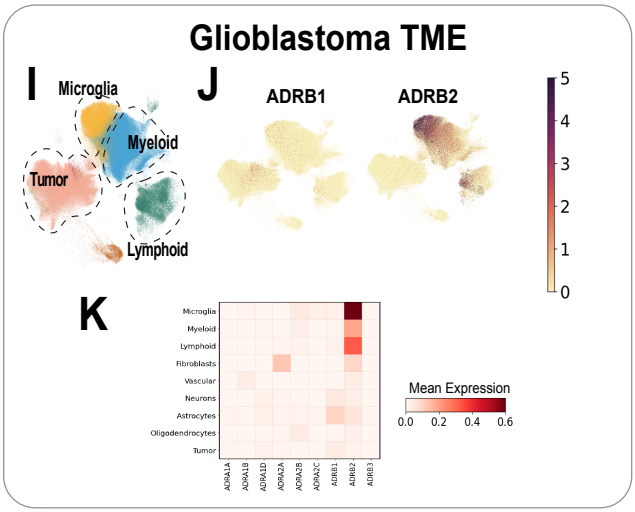

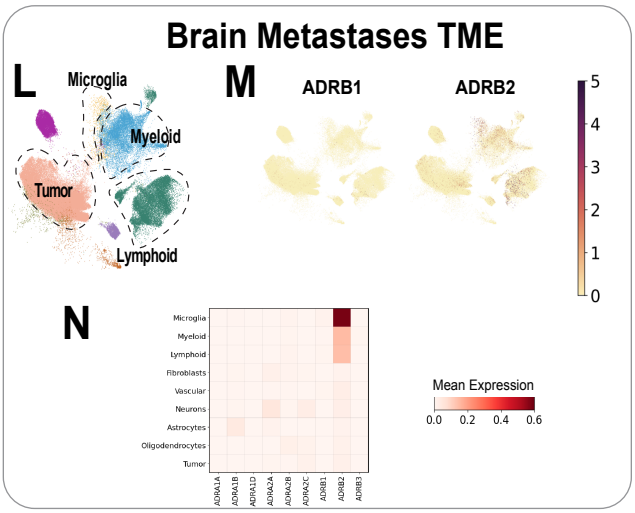

Figure 2. β-adrenergic receptors, not α-adrenergic receptors, are highly expressed on immune cells in the periphery and tumor microenvironment in humans. A. Integrated publicly available scRNAseq datasets from normal brain, glioblastoma, brain metastasis and PBMC samples. B. UMAP of clusters and cell types from integrated datasets. C. UMAP of clusters and cell types from healthy donor PBMCs. D. Feature plots of β1- and β2- adrenergic receptor expression in PBMCs from healthy donors. E. Heat map of β1- and β2- adrenergic receptor expression in healthy donor PBMC populations. F. UMAP of cluster and cell types from glioblastoma patient PBMCs. G. Feature plots of β1- and β2- adrenergic receptor expression in PBMCs from glioblastoma patients. H. Heat map of adrenergic receptor expression in glioblastoma PBMCs. I. UMAP of clusters and cell types glioblastoma tumor samples. J. Feature plots of β1- and β2- adrenergic receptor expression in the glioblastoma TME. K. Heat map of adrenergic receptor expression in various cell populations from the glioblastoma TME. L. UMAP of clusters and cell types from brain metastases samples. M. Feature plots of β1- and β2- adrenergic receptor expression in brain metastases TME. N. Heat map of adrenergic receptor expression in various cell types in the brain metastases TME.

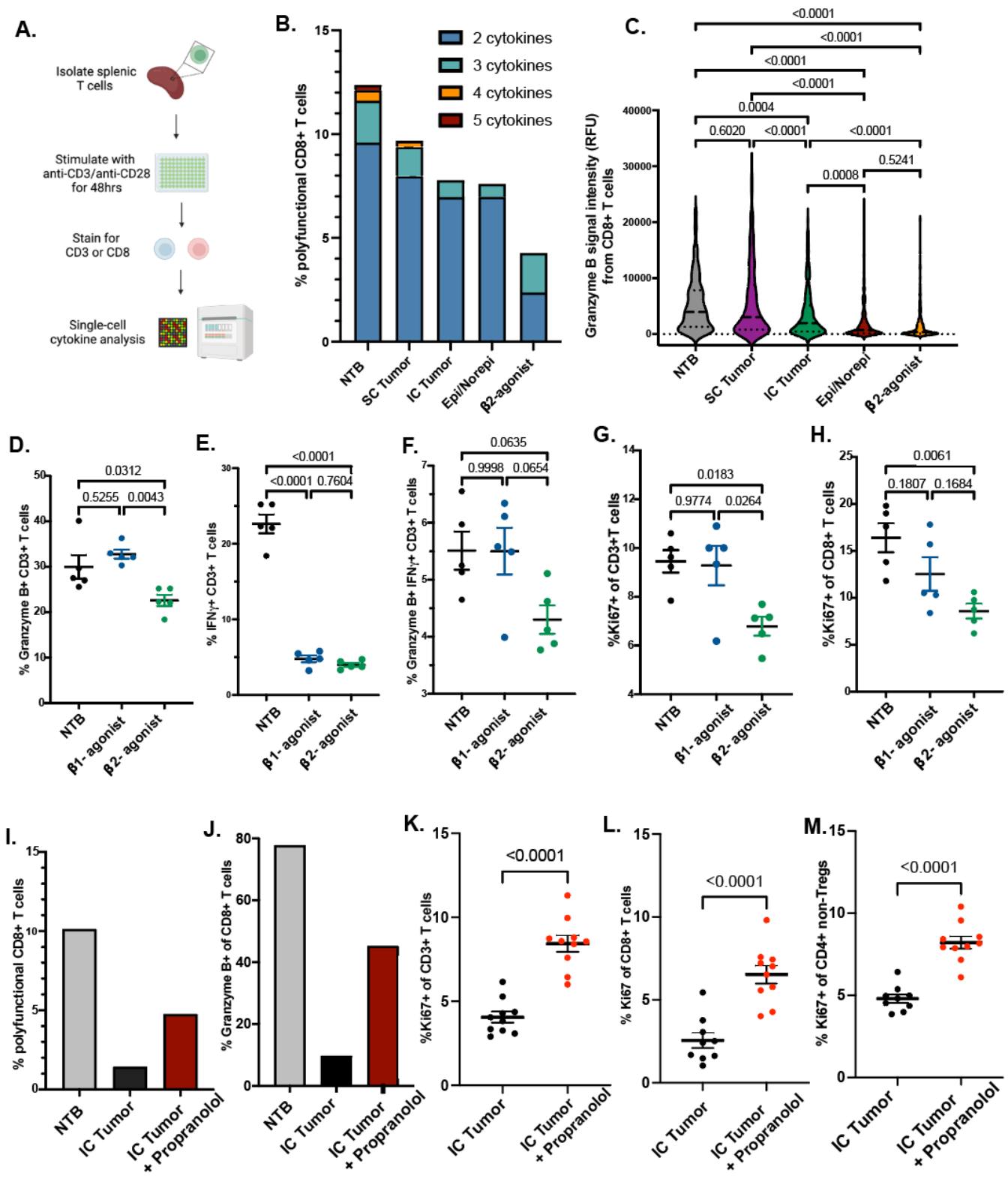

Figure 3. β-adrenergic signaling impairs systemic T cell function but β-adrenergic blockade restores function in the setting of intracranial tumors. A. Schematic of single-cell proteomics assay workflow (n=5 pooled mice per group for 30,000 total cells per chip). All intracranial tumor (IC tumor) mice were implanted with intracranial CT2A. All subcutaneous tumor (SC tumor) mice were implanted with subcutaneous CT2A. B. Proportion of $CD8^+$ T cells from each group that are polyfunctional (individual cells that secrete two or more cytokines). C. Granzyme B signal intensity in relative fluorescence units (RFU) plotted from all available raw data for $CD8^+$ T cells. Statistical significance was assessed using a one-way ANOVA with multiple comparisons. D,E. Flow cytometric analysis of non-tumor bearing (NTB) mice, or mice with subcutaneous pumps infusing dobutamine (β1-adrenergic agonist) or salbutamol (β2-adrenergic agonist). D,E. The percent of $CD3^+$ T cells secreting Granzyme B (D.) or IFNγ (E.). F. Percentage of polyfunctional $CD3^+$ T cells secreting both Granzyme B and IFNγ. G. Percentage of proliferating ($Ki67^+$) $CD3^+$ T cells. H. Percentage of proliferating ($Ki67^+$) $CD8^+$ T cells). Flow cytometric data reflect one experiment with n=5 mice. Statistical significance was assessed using a one-way ANOVA with multiple comparisons. I. Single-cell proteomics data demonstrating the percentage of $CD8^+$ T cells that secrete two or more cytokines in mice with no tumor, intracranial CT2A or intracranial CT2A treated with the non-selective β-adrenergic antagonist propranolol. J. Single-cell proteomics data demonstrating the percentage of $CD8^+$ T cells that secrete Granzyme B in mice with no tumor, intracranial CT2A or intracranial CT2A treated with propranolol. Flow cytometric analysis from mice with intracranial CT2A given no treatment or mice with intracranial CT2A treated with propranolol ; percentage of proliferating K. $CD3^+$ T cells L. $CD8^+$ T cells or M. $CD4^+$ non-Tregs. Panels K-M reflect at least two repeated experiments (n>9 mice per group). Statistical significance was assessed using unpaired t-tests.

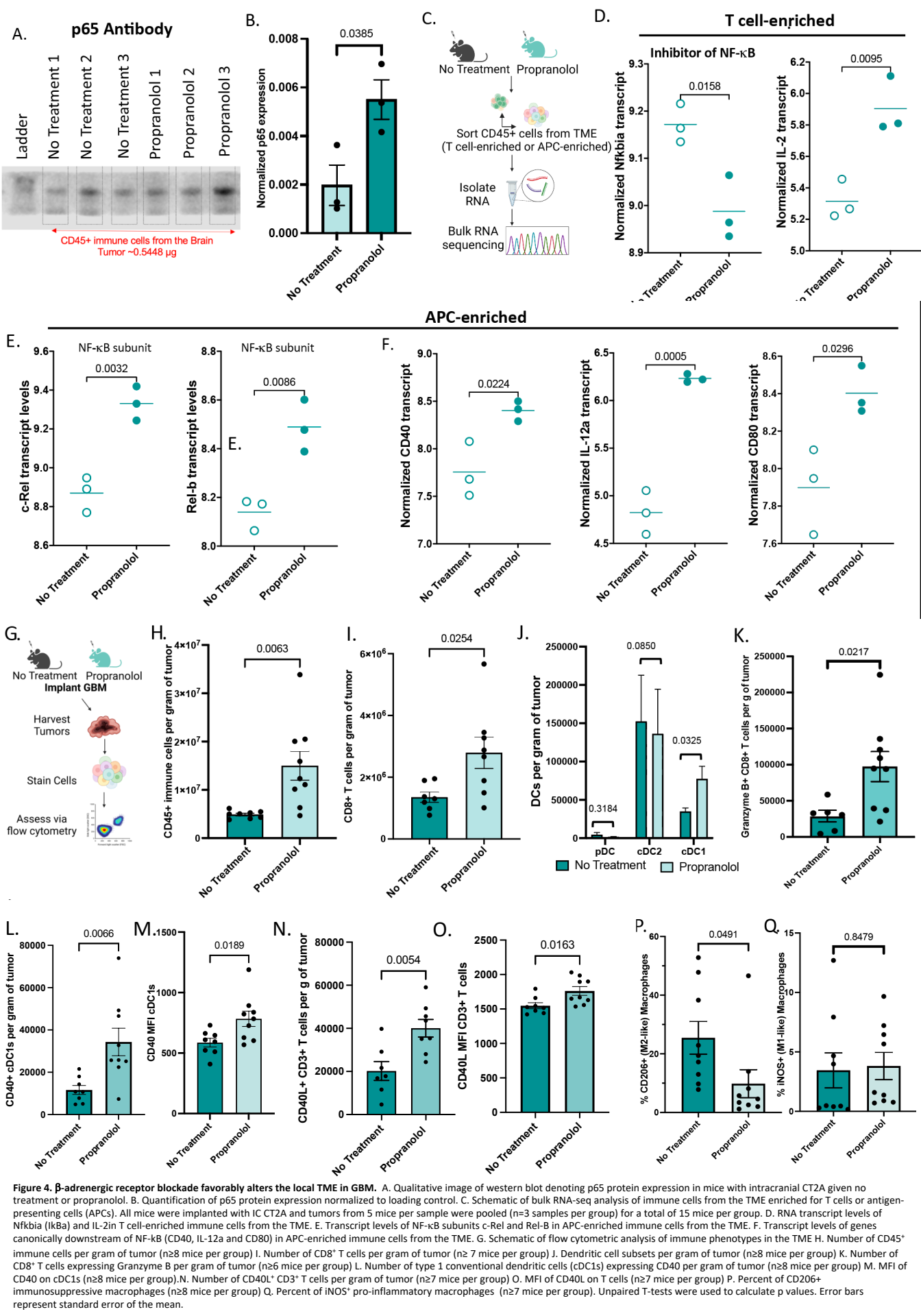

Figure 4. β-adrenergic receptor blockade favorably alters the local TME in GBM. A. Qualitative image of western blot denoting p65 protein expression in mice with intracranial CT2A given no treatment or propranolol. B. Quantification of p65 protein expression normalized to loading control. C. Schematic of bulk RNA-seq analysis of immune cells from the TME enriched for T cells or antigen-presenting cells (APCs). All mice were implanted with IC CT2A and tumors from 5 mice per sample were pooled (n=3 samples per group) for a total of 15 mice per group. D. RNA transcript levels of Nfkbia (IkBa) and IL-2in T cell-enriched immune cells from the TME. E. Transcript levels of NF-κB subunits c-Rel and Rel-B in APC-enriched immune cells from the TME. F. Transcript levels of genes canonically downstream of NF-kB (CD40, IL-12a and CD80) in APC-enriched immune cells from the TME. G. Schematic of flow cytometric analysis of immune phenotypes in the TME H. Number of CD45^{+} immune cells per gram of tumor (n≥8 mice per group) I. Number of CD8^{+} T cells per gram of tumor (n≥ 7 mice per group) J. Dendritic cell subsets per gram of tumor (n≥8 mice per group) K. Number of CD8^{+} T cells expressing Granzyme B per gram of tumor (n≥6 mice per group) L. Number of type 1 conventional dendritic cells (cDC1s) expressing CD40 per gram of tumor (n≥8 mice per group) M. MFI of CD40 on cDC1s (n≥8 mice per group).N. Number of CD40L^{+} CD3^{+} T cells per gram of tumor (n≥7 mice per group) O. MFI of CD40L on T cells (n≥7 mice per group) P. Percent of CD206+ immunosuppressive macrophages (n≥8 mice per group) Q. Percent of iNOS^{+} pro-inflammatory macrophages (n≥7 mice per group). Unpaired T-tests were used to calculate p values. Error bars represent standard error of the mean.

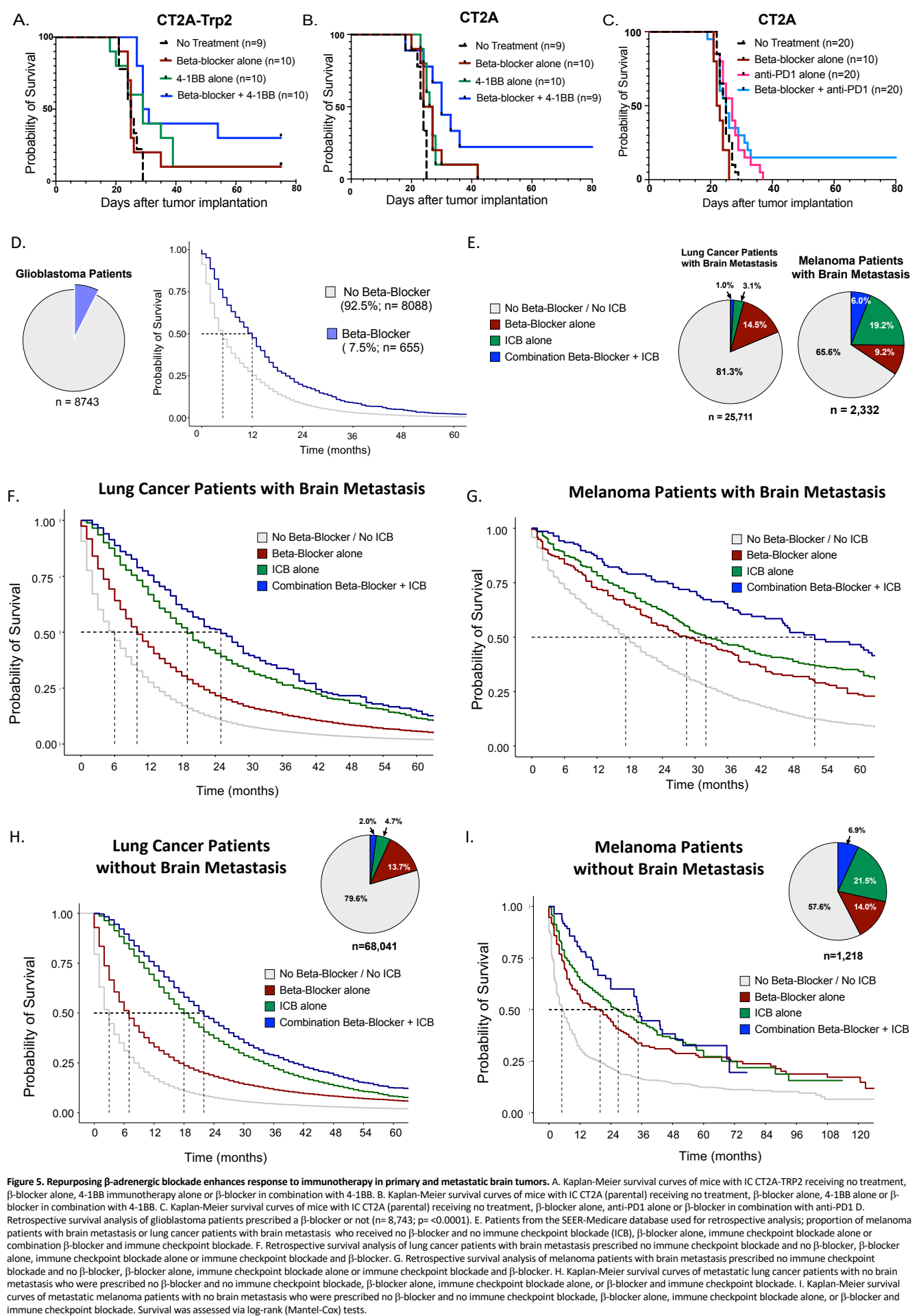

Figure 5. Repurposing β-adrenergic blockade enhances response to immunotherapy in primary and metastatic brain tumors. A. Kaplan-Meier survival curves of mice with IC CT2A-TRP2 receiving no treatment, β-blocker alone, 4-1BB immunotherapy alone or β-blocker in combination with 4-1BB. B. Kaplan-Meier survival curves of mice with IC CT2A (parental) receiving no treatment, β-blocker alone, 4-1BB alone or β-blocker in combination with 4-1BB. C. Kaplan-Meier survival curves of mice with IC CT2A (parental) receiving no treatment, β-blocker alone, anti-PD1 alone or β-blocker in combination with anti-PD1 D. Retrospective survival analysis of glioblastoma patients prescribed a β-blocker or not (n= 8,743; p= <0.0001). E. Patients from the SEER-Medicare database used for retrospective analysis; proportion of melanoma patients with brain metastasis or lung cancer patients with brain metastasis who received no β-blocker and no immune checkpoint blockade (ICB), β-blocker alone, immune checkpoint blockade alone or combination β-blocker and immune checkpoint blockade. F. Retrospective survival analysis of lung cancer patients with brain metastasis prescribed no immune checkpoint blockade and no β-blocker, β-blocker alone, immune checkpoint blockade alone or immune checkpoint blockade and β-blocker. G. Retrospective survival analysis of melanoma patients with brain metastasis prescribed no immune checkpoint blockade and no β-blocker, β-blocker alone, immune checkpoint blockade alone or immune checkpoint blockade and β-blocker. H. Kaplan-Meier survival curves of metastatic lung cancer patients with no brain metastasis who were prescribed no β-blocker and no immune checkpoint blockade, β-blocker alone, immune checkpoint blockade alone, or β-blocker and immune checkpoint blockade. I. Kaplan-Meier survival curves of metastatic melanoma patients with no brain metastasis who were prescribed no β-blocker and no immune checkpoint blockade, β-blocker alone, immune checkpoint blockade alone, or β-blocker and immune checkpoint blockade. Survival was assessed via log-rank (Mantel-Cox) tests.

Table 1. Demographics and Survival Data from Glioblastoma Patients in SEER-Medicare 2008-2017

1.1. Overall

Characteristic	N = 8,743[1]
Patient Age	74 (69, 80)
Sex	
M	4,699 (54%)
F	4,044 (46%)
Race/ethnicity	
NH White	7,572 (87%)
NH Black	307 (3.5%)
NH Other	315 (3.6%)
Hispanic	549 (6.3%)
Charlson score	
0	4,654 (53%)
1	1,854 (21%)
2	1,049 (12%)
3+	1,186 (14%)
Received radiation	
None	3,347 (38%)
Yes	5,396 (62%)
Received chemotherapy	
None/Unknown	2,802 (44%)
Yes	3,591 (56%)
Unknown	2,350
Received surgery of primary	
None	2,411 (28%)
Yes	6,332 (72%)
Any betablocker	
No betablocker	8,088 (93%)

Characteristic	N = 8,743[1]
Betablocker	655 (7.5%)

[1]Median (IQR); n (%)

1.2. Median Survival Months

Characteristic	Median Survival
Any betablocker	
No betablocker	5.0 (5.0, 5.0)
Betablocker	12 (11, 13)

1.3. Adjusted Survival Model

Characteristic	HR[1]	95% CI[1]	p-value
Patient Age	1.02	1.02, 1.03	**<0.001**
Sex			
M	—	—	
F	1.00	0.95, 1.05	0.920
Race/ethnicity			
NH White	—	—	
NH Black	0.77	0.67, 0.88	**<0.001**
NH Other	0.74	0.66, 0.84	**<0.001**
Hispanic	0.95	0.86, 1.05	0.282
Charlson score			
0	—	—	
1	1.14	1.07, 1.22	**<0.001**
2	1.28	1.18, 1.39	**<0.001**
3+	1.41	1.30, 1.52	**<0.001**
Received radiation			
None	—	—	
Yes	0.56	0.52, 0.60	**<0.001**
Received chemotherapy			
None/Unknown	—	—	
Yes	0.56	0.52, 0.60	**<0.001**

Characteristic	HR[1]	95% CI[1]	p-value
Received surgery of primary			
None	—	—	
Yes	0.62	0.59, 0.66	**<0.001**
Any betablocker			
No betablocker	—	—	
Betablocker	0.63	0.57, 0.69	**<0.001**

[1]HR = Hazard Ratio, CI = Confidence Interval

Table 2. Demographics and Survival Data of Metastatic Lung Cancer Patients with Brain Metastasis in SEER-Medicare 2008-2017

2.1 Overall

Characteristic	N = 25,711[1]
Patient Age	73 (68, 78)
Sex	
M	12,485 (49%)
F	13,226 (51%)
Race/ethnicity	
NH White	20,813 (81%)
Hispanic	1,224 (4.8%)
NH Black	1,993 (7.8%)
NH Other	1,681 (6.5%)
Charlson score	
0	11,288 (44%)
1	7,148 (28%)
2	3,542 (14%)
3+	3,733 (15%)
Received radiation	
None	9,359 (36%)
Yes	16,352 (64%)
Received chemotherapy	
None	15,137 (59%)
Yes	10,574 (41%)
Received surgery of primary	
None	23,736 (92%)
Yes	1,975 (7.7%)
LC subtype	
NSCLC	20,326 (79%)
SCLC	5,385 (21%)

Characteristic	N = 25,711[1]
Betablocker and checkpoint inhibitor use	
No betablocker/No ICB	20,905 (81%)
Betablocker only	3,733 (15%)
ICB only	806 (3.1%)
Betablocker and ICB	267 (1.0%)

[1]Median (IQR); n (%)

2.2 Pairwise Log-rank P-values

Treatment	No betablocker/No ICB	Betablocker only	ICB only
Betablocker only	<0.001		
ICB only	<0.001	<0.001	
Betablocker and ICB	<0.001	<0.001	0.013

n: 3

2.3 Median Survival Months

Characteristic	Median Survival
Betablocker and checkpoint inhibitor use	
No betablocker/No ICB	6.0 (5.0, 6.0)
Betablocker only	10 (10, 11)
ICB only	19 (18, 21)
Betablocker and ICB	25 (22, 29)

2.4 Adjusted Survival Model

Characteristic	HR[1]	95% CI[1]	p-value
Patient Age	1.02	1.01, 1.02	**<0.001**
Sex			
M	—	—	
F	0.83	0.81, 0.85	**<0.001**
Race/ethnicity			
NH White	—	—	
Hispanic	0.97	0.92, 1.03	0.351

Characteristic	HR[1]	95% CI[1]	p-value
NH Black	1.02	0.97, 1.07	0.481
NH Other	0.79	0.75, 0.84	**<0.001**
Charlson score			
0	—	—	
1	1.04	1.01, 1.07	**0.021**
2	1.07	1.03, 1.11	**<0.001**
3+	1.17	1.13, 1.22	**<0.001**
Received radiation			
None	—	—	
Yes	0.76	0.74, 0.78	**<0.001**
Received chemotherapy			
None	—	—	
Yes	0.65	0.63, 0.67	**<0.001**
Received surgery of primary			
None	—	—	
Yes	0.32	0.31, 0.34	**<0.001**
LC subtype			
NSCLC	—	—	
SCLC	0.97	0.94, 1.00	0.075
Betablocker and checkpoint inhibitor use			
No betablocker/No ICB	—	—	
Betablocker only	0.65	0.63, 0.67	**<0.001**
ICB only	0.46	0.43, 0.50	**<0.001**
Betablocker and ICB	0.37	0.32, 0.43	**<0.001**

[1]HR = Hazard Ratio, CI = Confidence Interval

Table 3. Demographics and Survival Data from Metastatic Melanoma Patients with Brain Metastasis in SEER-Medicare 2008-2017

3.1. Overall

Characteristic	N = 2,332[1]
Patient Age	74 (69, 81)
Sex	
Male	1,606 (69%)
Female	726 (31%)
Race/ethnicity	
NH White	2,216 (95%)
Hispanic	66 (2.8%)
NH Black	22 (0.9%)
NH Other	28 (1.2%)
Charlson score	
0	1,327 (57%)
1	335 (14%)
2	362 (16%)
3+	308 (13%)
Received radiation	
None	1,473 (63%)
Yes	859 (37%)
Received chemotherapy	
None	1,323 (57%)
Yes	1,009 (43%)
Received surgery of primary	
None	819 (35%)
Yes	1,513 (65%)
Betablocker and checkpoint inhibitor use	
No betablocker/No ICB	1,531 (66%)
Betablocker only	215 (9.2%)
ICB only	447 (19%)
Betablocker and ICB	139 (6.0%)

[1]Median (IQR); n (%)

3.2. Pairwise Log-rank P-values

Treatment	No betablocker/No ICB	Betablocker only	ICB only
Betablocker only	<0.001		
ICB only	<0.001	0.066	
Betablocker and ICB	<0.001	<0.001	0.006

n: 3

3.3. Median Survival Months

Characteristic	Median Survival
Betablocker and checkpoint inhibitor use	
No betablocker/No ICB	17 (16, 19)
Betablocker only	28 (23, 37)
ICB only	32 (29, 39)
Betablocker and ICB	52 (46, 70)

3.4. Adjusted Survival Model

Characteristic	HR[1]	95% CI[1]	p-value
Patient Age	1.02	1.01, 1.02	**<0.001**
Sex			
Male	—	—	
Female	0.90	0.81, 0.99	**0.029**
Race/ethnicity			
NH White	—	—	
Hispanic	1.06	0.81, 1.39	0.675
NH Black	0.87	0.56, 1.36	0.547
NH Other	0.81	0.54, 1.22	0.323
Charlson score			

Characteristic	HR[1]	95% CI[1]	p-value
0	—	—	
1	1.08	0.95, 1.24	0.236
2	1.14	1.00, 1.30	**0.043**
3+	1.33	1.16, 1.53	**<0.001**
Received radiation			
None	—	—	
Yes	1.44	1.30, 1.58	**<0.001**
Received chemotherapy			
None	—	—	
Yes	0.72	0.65, 0.81	**<0.001**
Received surgery of primary			
None	—	—	
Yes	0.47	0.43, 0.52	**<0.001**
Betablocker and checkpoint inhibitor use			
No betablocker/No ICB	—	—	
Betablocker only	0.54	0.46, 0.63	**<0.001**
ICB only	0.56	0.49, 0.65	**<0.001**
Betablocker and ICB	0.40	0.31, 0.50	**<0.001**

[1] HR = Hazard Ratio, CI = Confidence Interval

Table 4. Demographics and Survival Data from Metastatic Lung Cancer Patients with no Brain Metastasis in SEER-Medicare 2008-2017

4.1. Overall

Characteristic	N = 68,041[1]
Patient Age	75 (70, 82)
Sex	
M	35,460 (52%)
F	32,581 (48%)
Race/ethnicity	
NH White	55,636 (82%)
Hispanic	3,111 (4.6%)
NH Black	5,072 (7.5%)
NH Other	4,222 (6.2%)
Charlson score	
0	26,473 (39%)
1	16,693 (25%)
2	10,279 (15%)
3+	14,596 (21%)
Received radiation	
None	48,198 (71%)
Yes	19,843 (29%)
Received chemotherapy	
None	46,061 (68%)
Yes	21,980 (32%)
Received surgery of primary	
None	65,667 (97%)
Yes	2,374 (3.5%)
LC subtype	
NSCLC	57,339 (84%)
SCLC	10,702 (16%)

Characteristic	N = 68,041[1]
Betablocker and checkpoint inhibitor use	
No betablocker/No ICB	54,149 (80%)
Betablocker only	9,296 (14%)
ICB only	3,197 (4.7%)
Betablocker and ICB	1,399 (2.1%)

[1]Median (IQR); n (%)

4.2. Pairwise Log-rank P-values

Treatment	No betablocker/No ICB	Betablocker only	ICB only
Betablocker only	<0.001		
ICB only	<0.001	<0.001	
Betablocker and ICB	<0.001	<0.001	<0.001

n: 3

4.3. Median Survival Months

Characteristic	Median Survival
Betablocker and checkpoint inhibitor use	
No betablocker/No ICB	3.0 (3.0, 3.0)
Betablocker only	7.0 (7.0, 7.0)
ICB only	18 (18, 19)
Betablocker and ICB	22 (21, 24)

Characteristic	HR	95% CI	p-value
Patient Age	1.01	1.01, 1.01	**<0.001**
Sex			
M	—	—	

F	0.86	0.85, 0.88	**<0.001**
Race/ethnicity			
NH White	—	—	
Hispanic	0.93	0.90, 0.97	**<0.001**
	[1]	[1]	

1.4. Adjusted Survival Model

Characteristic	HR[1]	95% CI[1]	p-value
NH Black	1.03	1.00, 1.06	0.096
NH Other	0.80	0.78, 0.83	**<0.001**
Charlson score			
0	—	—	
1	1.10	1.07, 1.12	**<0.001**
2	1.19	1.16, 1.22	**<0.001**
3+	1.38	1.36, 1.42	**<0.001**
Received radiation			
None	—	—	
Yes	0.67	0.66, 0.68	**<0.001**
Received chemotherapy			
None	—	—	
Yes	0.59	0.58, 0.60	**<0.001**
Received surgery of primary			
None	—	—	
Yes	0.37	0.36, 0.39	**<0.001**

[1] HR = Hazard Ratio, CI = Confidence Interval

LC subtype			
NSCLC	—	—	
SCLC	1.33	1.30, 1.36	**<0.001**
Betablocker and checkpoint inhibitor use			
No betablocker/No ICB	—	—	
Betablocker only	0.59	0.57, 0.60	**<0.001**
ICB only	0.41	0.40, 0.43	**<0.001**
Betablocker and ICB	0.34	0.32, 0.36	**<0.001**

Table 5. Demographics and Survival Data from Metastatic Melanoma Patients with no Brain Metastasis in SEER-Medicare 2008-2017

5.1. Overall

Characteristic	N = 1,218[1]
Patient Age	77 (70, 84)
Sex	
Male	797 (65%)
Female	421 (35%)
Race/ethnicity	
NH White	1,139 (94%)
Hispanic	42 (3.4%)
NH Black	18 (1.5%)
NH Other	19 (1.6%)
Charlson score	
0	660 (54%)
1	174 (14%)
2	171 (14%)
3+	213 (17%)
Received radiation	
None	1,022 (84%)
Yes	196 (16%)
Received chemotherapy	
None	759 (62%)
Yes	459 (38%)
Received surgery of primary	
None	751 (62%)
Yes	467 (38%)
Betablocker and checkpoint inhibitor use	
No betablocker/No ICB	702 (58%)
Betablocker only	170 (14%)
ICB only	262 (22%)
Betablocker and ICB	84 (6.9%)

[1]Median (IQR); n (%)

5.2. Pairwise Log-rank P-values

Treatment	No betablocker/No ICB	Betablocker only	ICB only
Betablocker only	<0.001		
ICB only	<0.001	0.165	
Betablocker and ICB	<0.001	0.019	0.158

n: 3

5.3. Median Survival Months

Characteristic	Median Survival
Betablocker and checkpoint inhibitor use	
No betablocker/No ICB	5.0 (4.0, 6.0)
Betablocker only	20 (12, 26)
ICB only	27 (21, 38)
Betablocker and ICB	35 (24, 52)

5.4. Adjusted Survival Model

Characteristic	HR[1]	95% CI[1]	p-value
Patient Age	1.02	1.01, 1.03	**<0.001**
Sex			
Male	—	—	
Female	1.01	0.88, 1.16	0.878
Race/ethnicity			
NH White	—	—	
Hispanic	0.84	0.58, 1.21	0.358
NH Black	1.30	0.79, 2.15	0.299
NH Other	1.34	0.83, 2.14	0.229
Charlson score			

Characteristic	HR[1]	95% CI[1]	p-value
0	—	—	
1	1.20	0.98, 1.47	0.072
2	1.29	1.06, 1.58	**0.013**
3+	1.56	1.30, 1.86	**<0.001**
Received radiation			
None	—	—	
Yes	0.94	0.79, 1.12	0.470
Received chemotherapy			
None	—	—	
Yes	0.61	0.50, 0.75	**<0.001**
Received surgery of primary			
None	—	—	
Yes	0.59	0.52, 0.68	**<0.001**
Betablocker and checkpoint inhibitor use			
No betablocker/No ICB	—	—	
Betablocker only	0.50	0.41, 0.61	**<0.001**
ICB only	0.68	0.54, 0.86	**0.002**
Betablocker and ICB	0.53	0.37, 0.74	**<0.001**

[1] HR = Hazard Ratio, CI = Confidence Interval